Supporting Information

Ratiometric Luminescence Sensing of Bio-Macromolecules via Highly Sensitive Templated Pyrene-Based nanoGUMBOS

Rajkumar Sahoo[a], Prabal Pramanik[a], Sudhir Kumar Das[b], and Mintu Halder[a], *

[a] Department of Chemistry, Indian Institute of Technology Kharagpur, Kharagpur,721302, India.

[b] Department of Chemistry, University of North Bengal, Darjeeling,734013, India

E-mail: mintu@chem.iitkgp.ac.in

Instrumental details:

UV−vis and fluorescence spectra

Steady-state UV−Vis and fluorescence spectra were recorded with a Shimadzu UV-2600 spectrophotometer and Horiba Fluorolog-3 spectrofluorometer, respectively. For spectroscopic measurements, freshly prepared nanoGUMBOS solution (mostly 20 μg/mL) was used. The vertical line with caps on the data points in any plot represents error bar.

Time-resolved photoluminescence

The time-resolved photoluminescence lifetime decays are measured by a time-correlated single photon counting (TCSPC) picosecond spectrophotometer (LifeSpec II, Edinburgh Instruments, U.K.) with the help of different excitation laser sources indicated accordingly. The emissions were collected by using a Micro Channel Plate PMT detector (Hammamatsu MCP PMT Air cooled, Model-3809U-50). For the determination of instrument response function (IRF), we have used colloidal Ludox solution.

FTIR and DLS.

Fourier transform infrared spectroscopic measurements were done with Perkin- Elmer FTIR spectrophotometer, Model: Spectrum Two.

The size distribution of particles is measured by dynamic light scattering (DLS; Malvern Nano ZS instrument) using a 4 mW He−Ne laser (λ= 632.8 nm). The zeta potential (ζ) of nanoparticles is also obtained by this instrument using a capillary ζ-cell.

CD measurement:

CD spectra were recorded on a Jasco-1500 automatic recording spectropolarimeter at 298 K at a scan speed of 50 nm/min by averaging three successive scans over a wavelength range of 250-450 nm. A quartz cell was used having a path length of 1 cm and for baseline correction Millipore water used.

Differential scanning calorimetry (DSC):

Differential scanning calorimetric (DSC) study was performed by Thermal Analysis (DSC Q20) instrument using a Tzero aluminium pan with a scan rate of 10 ºC min^{-1} in the range of -50 ºC to 250 ºC under a nitrogen atmosphere.

FESEM and TEM:

FE-SEM images were collected using a ZESSI instrument working at 5KV. The film samples were drop casted on a glass slide and gold coated for imaging. Transmission electron microscopy (JEOL TEM-2010) is used for determining the morphology of the nanoparticles with an operating voltage of 200 kV. The average particle size has been obtained by measuring the size of more than 100 particles. Energy dispersive X-ray spectroscopy (EDX) measurement is carried out for elemental analysis. For TEM study, a small aliquot of aqueous solution of nPBIL and nPBTOP (20 μg/mL) has been drop casted on carbon coated copper grids.

Docking Studies

The available crystal structures of Heparin (PDB ID: 1hpn) in the protein data bank were used for docking studies. To evaluate the possible binding modes, we use the Auto Dock Vina and Auto Dock Tools, using the 3-D crystal structure of Heparin. AutoDock-1.5.7 uses the Lamarckian genetic algorithm to find out the different conformations of small molecules in the biomolecule. The most favourable docking conformation was chosen based on their lowest binding energy. The docking of pyrene butyrate (PB) (ligand) was done on the structure of heparin(receptor) (1:1). An additional PB molecule was docked onto the structure of PB-Heparin upon selection of the energetically best-docked configuration from the system to further obtain the best-docked configuration of PB/heparin (2:1) system. The docking was performed with the center grid maintained at -8.1, -8.7, -1.8 concerning the heparin axis, 0.5 Å grid spacing, and x, y, and z coordinates of 40.8, 40.3, and 24.8, respectively. The docked conformation was visualized by using BIOVIA Discovery Studio.

Preparation of solution:

Preparation of GUMBOS solution:

Initially, stock solution of GUMBOS was prepared by dissolving the sticky solid in spectroscopic grade tetrahydro furan (THF). Then prepared 20 μg/mL nanoGUMBOS solution in aqueous media using the stock solution of THF. Solutions of GUMBOS in aqueous medium were equilibrated for 10 mins before each experiment.

Preparation of serum albumin solution:

The stock solution of human serum albumin was diluted to 20 % with phosphate buffer solution (10 mM, pH 7.4) and then introduced into it a 20 μg/mL nanoGUMBOS solution. Then various concentration of heparin stock solution was added to the diluted serum albumin solution, and

then the total volume of the test solution was adjusted to 2 mL by using the diluted serum solution. After incubation for 10 min at room temperature, the test solution was subjected to fluorescence determination under 350 nm excitation.

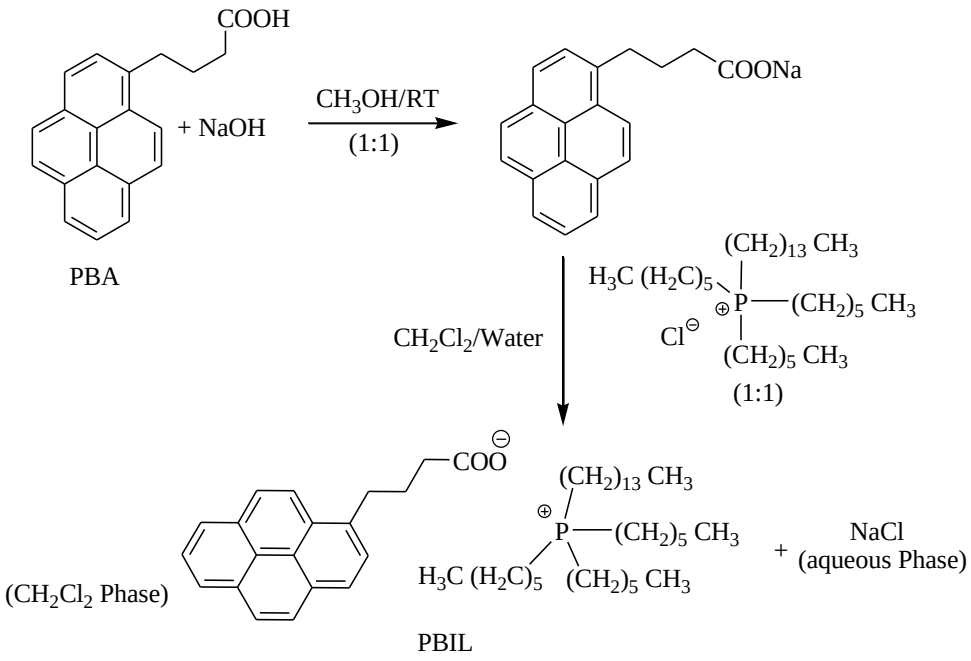

Scheme. S1 Synthetic route for the preparation of PBIL

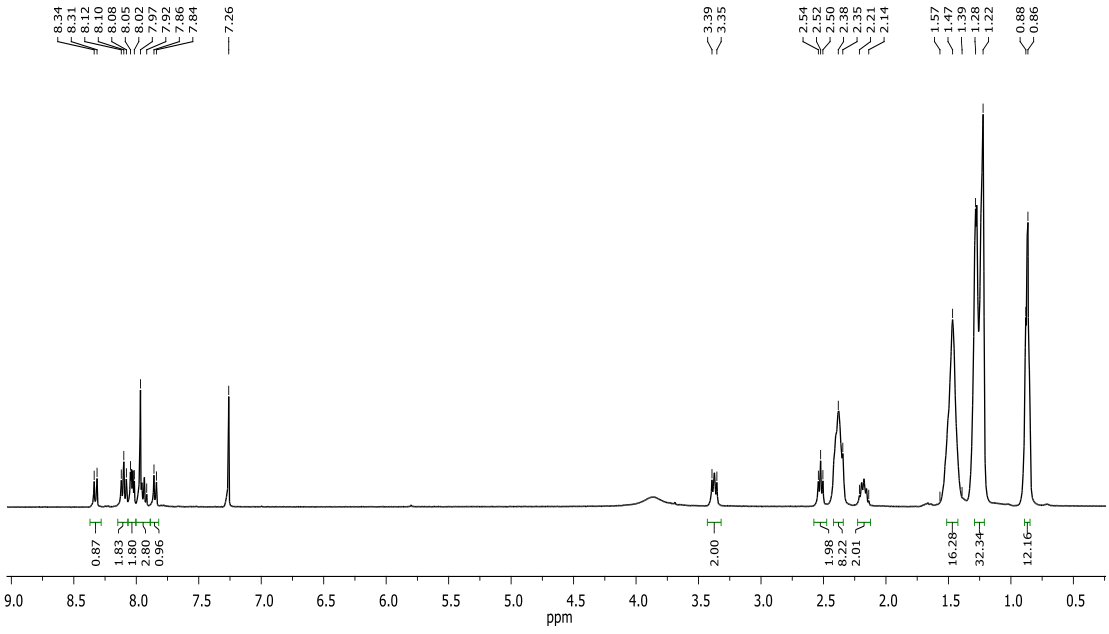

Figure. S1 ^{1}H NMR spectrum ($CDCl_3$, 400 MHz) of PBIL

^{1}H NMR (400 MHz, $CDCl_3$): δ (ppm) 8.33 (d, *J* = 9.2 Hz, 1H), 8.10 (t, *J* = 8.2 Hz, 2H), 8.06 – 8.02 (m, 2H), 7.97 – 7.92 (m, 3H), 7.85 (d, *J* = 7.8 Hz, 1H), 3.39 – 3.35 (m, 2H), 2.52 (t, *J* = 7.2 Hz, 2H), 2.38 – 2.35 (m, 8H), 2.21 – 2.24 (m, 2H), 1.57 – 1.39 (m, 16H), 1.28 – 1.22 (m, 32H), 0.88 – 0.86 (m, 12H).

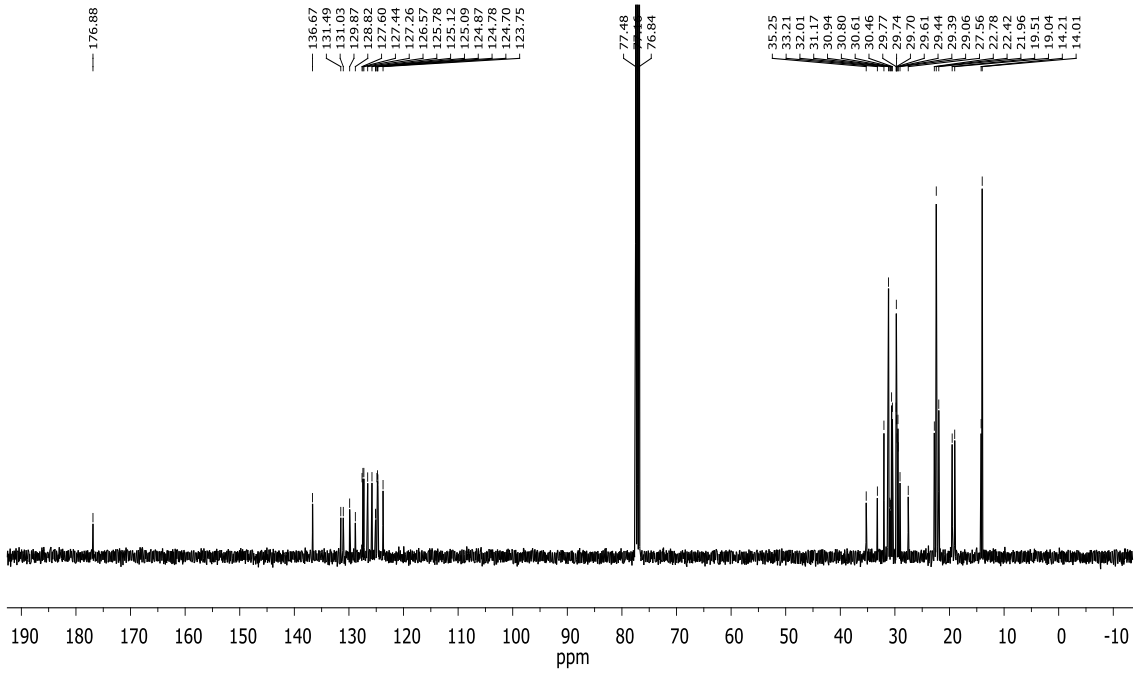

Figure. S2 ^{13}C NMR spectrum ($CDCl_3$, 100 MHz) of PBIL.

^{13}C NMR (100 MHz, $CDCl_3$): δ (ppm) 176.9, 136.7, 131.5, 131.0, 129.9, 128.8, 127.6, 127.4, 127.3, 126.6, 125.8, 125.1, 125.1, 124.9, 124.8, 124.7, 123.8, 35.3, 33.2, 32.0, 31.2, 30.9, 30.8, 30.6, 30.5, 29.8, 29.7, 29.7, 29.6, 29.4, 29.4, 29.1, 27.6, 22.8, 22.4, 22.0, 19.5, 19.0, 14.2, 14.0.

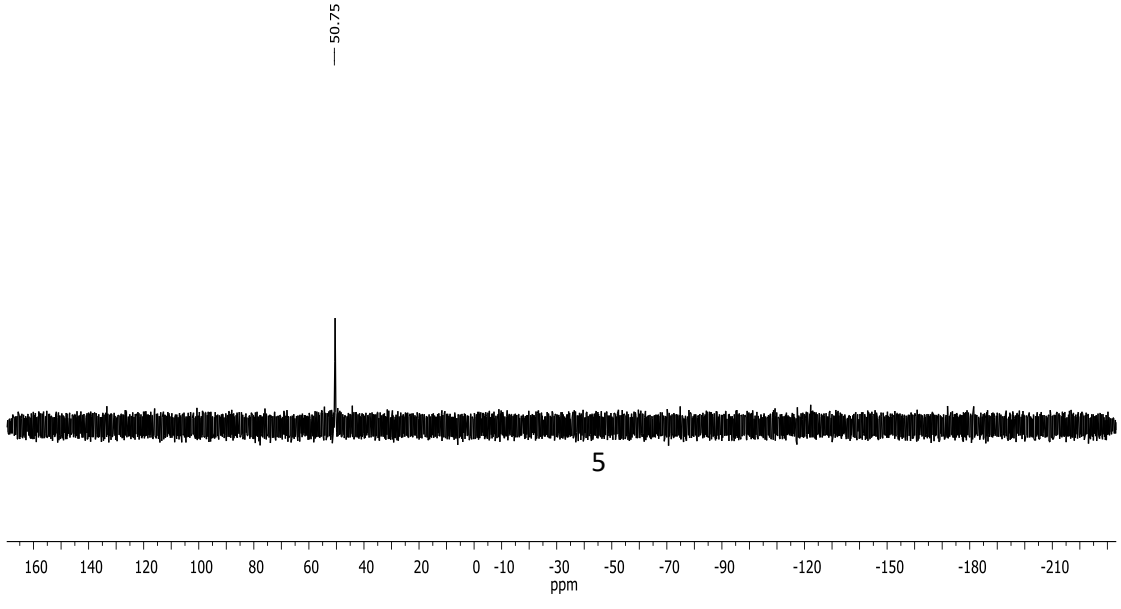

Figure. S3 ^{31}P NMR spectrum ($CDCl_3$, 202 MHz) of PBIL.

^{31}P NMR (202 MHz, $CDCl_3$): δ (ppm) 50.75.

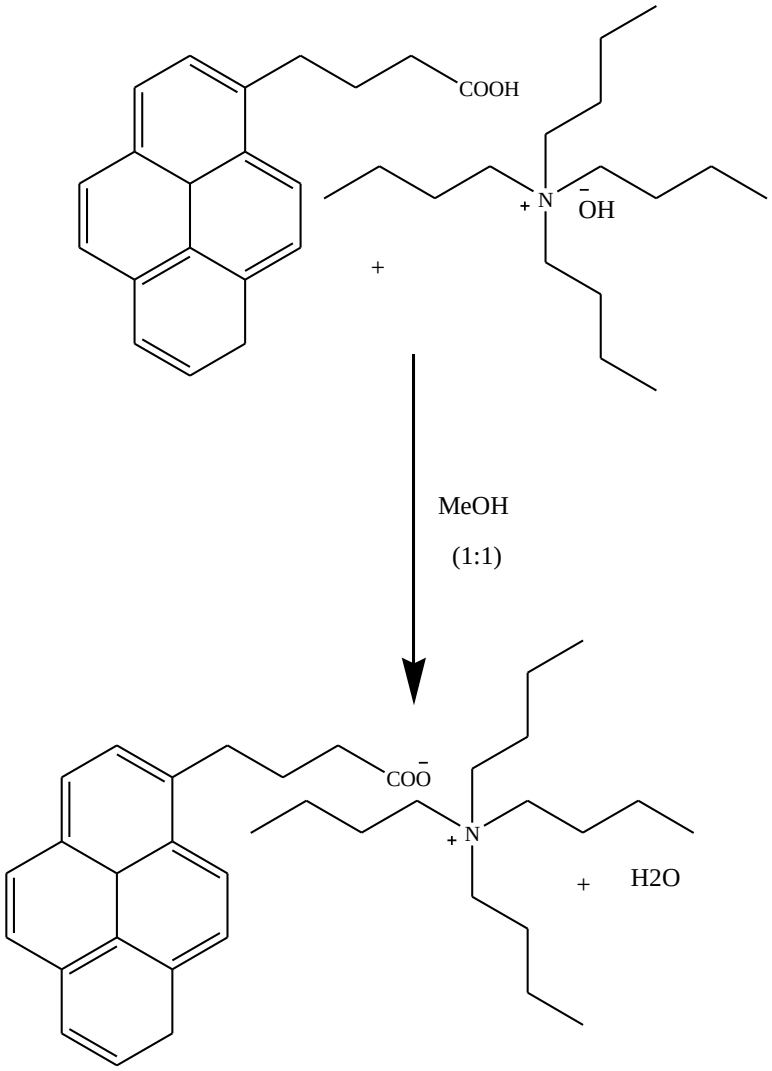

Scheme. S2 Synthetic route for the preparation of PBTBA

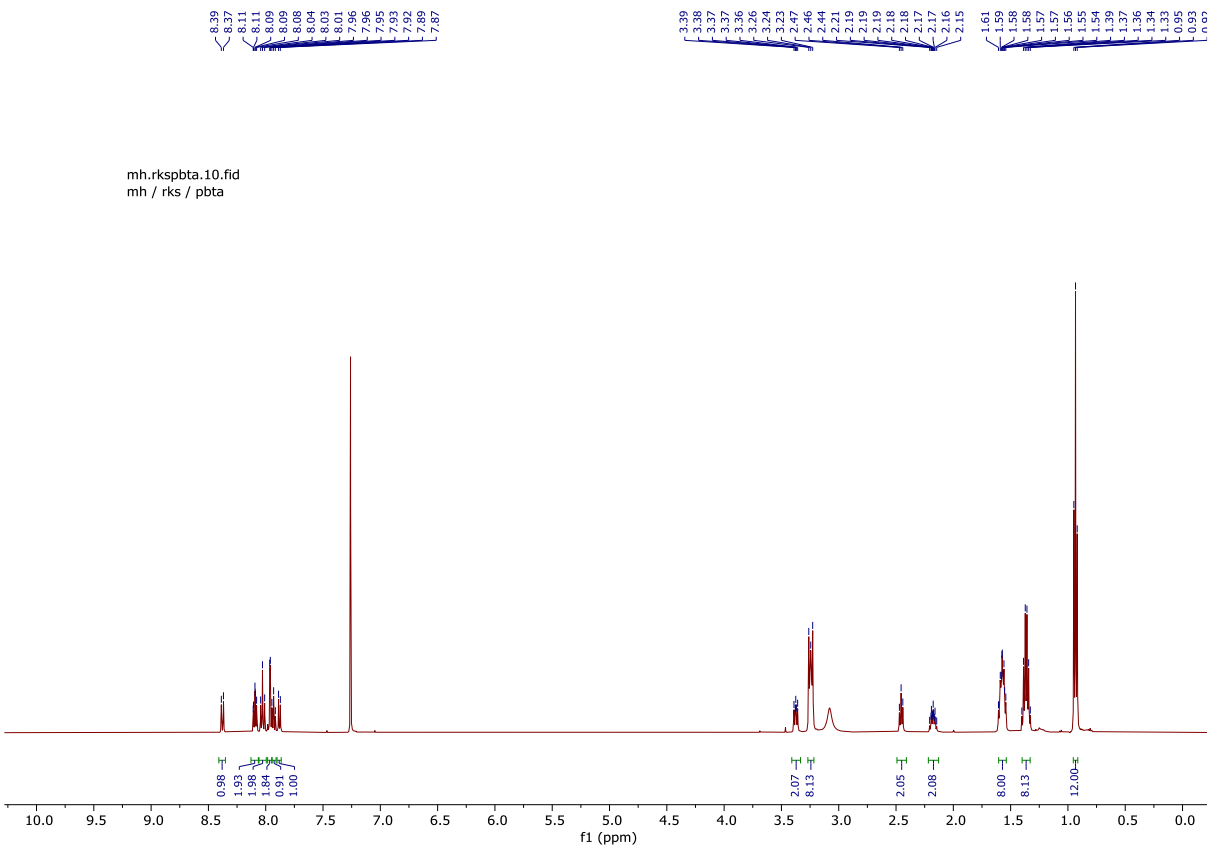

Figure. S4 ^{1}H NMR spectrum ($CDCl_3$, 500 MHz) of PBTBA

^{1}H NMR (500 MHz, Chloroform-*d*) δ 8.38 (d, *J* = 9.2 Hz, 1H), 8.09 (dd, *J* = 7.4, 6.1 Hz, 2H), 8.03 (t, *J* = 8.7 Hz, 2H), 7.96 (d, *J* = 2.5 Hz, 2H), 7.92 (d, *J* = 7.6 Hz, 1H), 7.88 (d, *J* = 7.8 Hz, 1H), 3.41 – 3.33 (m, 2H), 3.27 – 3.22 (m, 8H), 2.46 (t, *J* = 7.4 Hz, 2H), 2.18 (tt, *J* = 10.1, 6.6 Hz, 2H), 1.57 (qd, *J* = 8.1, 7.7, 4.7 Hz, 8H), 1.36 (q, *J* = 7.4 Hz, 8H), 0.93 (t, *J* = 7.4 Hz, 12H).

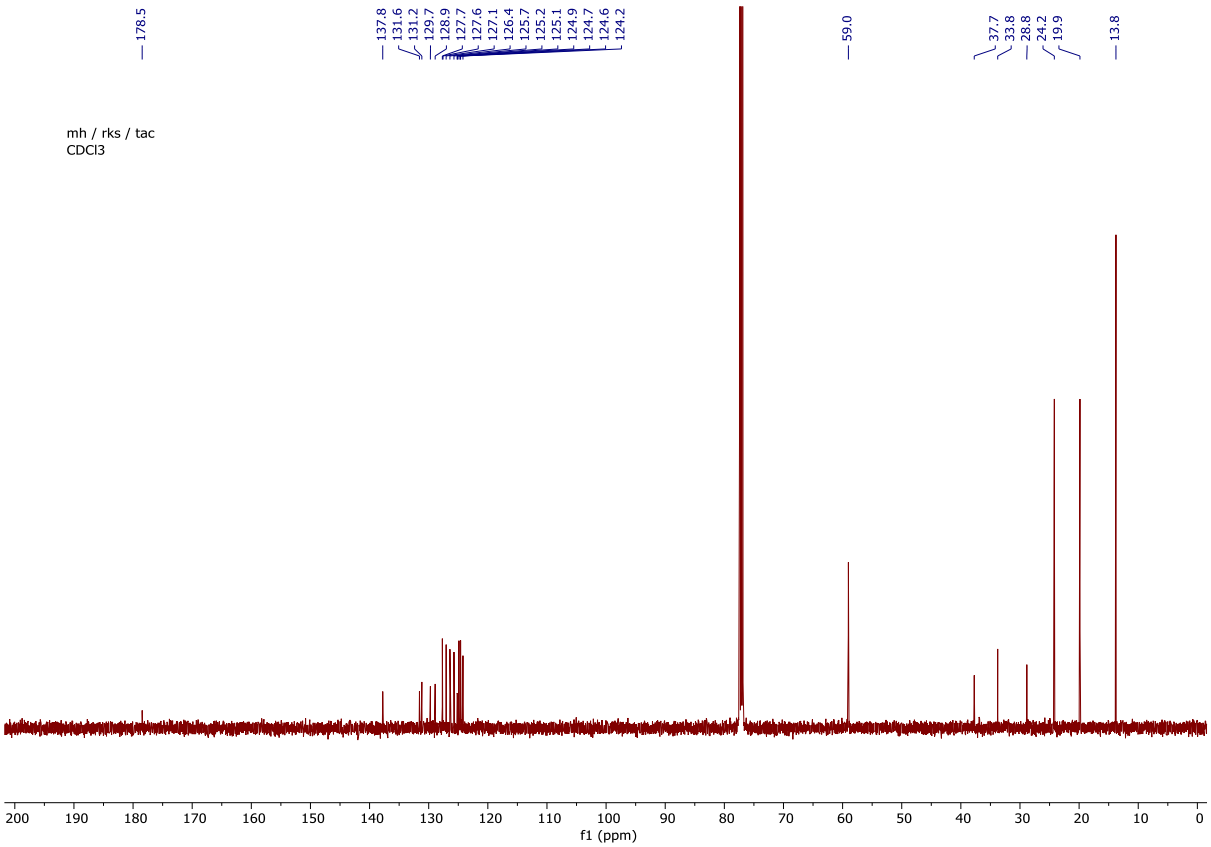

Figure. S5 ^{13}C NMR spectrum ($CDCl_3$, 500 MHz) of PBTBA

^{13}C NMR (126 MHz, $CDCl_3$) δ 178.46, 137.77, 131.56, 131.16, 129.71, 128.91, 127.69, 127.58, 127.05, 126.41, 125.73, 125.19, 125.14, 124.88, 124.65, 124.61, 124.20, 59.02, 37.73, 33.77, 28.84, 24.19, 19.86, 13.77.

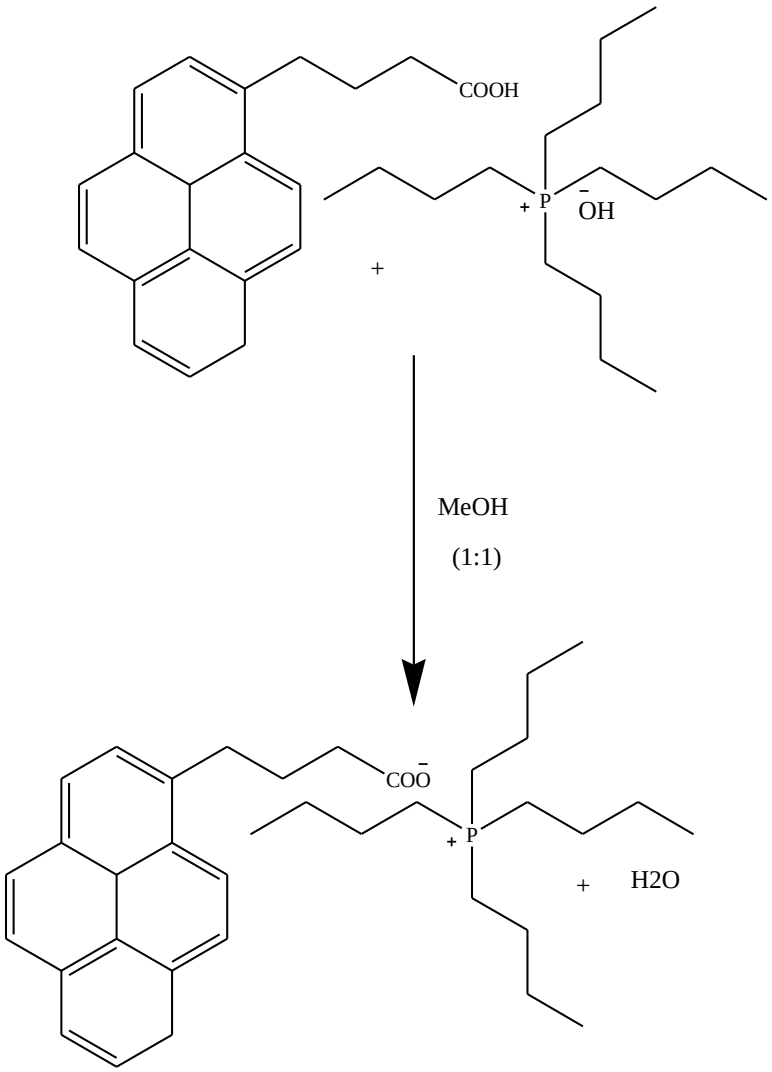

Scheme. S3 Synthetic route for the preparation of PBTBP

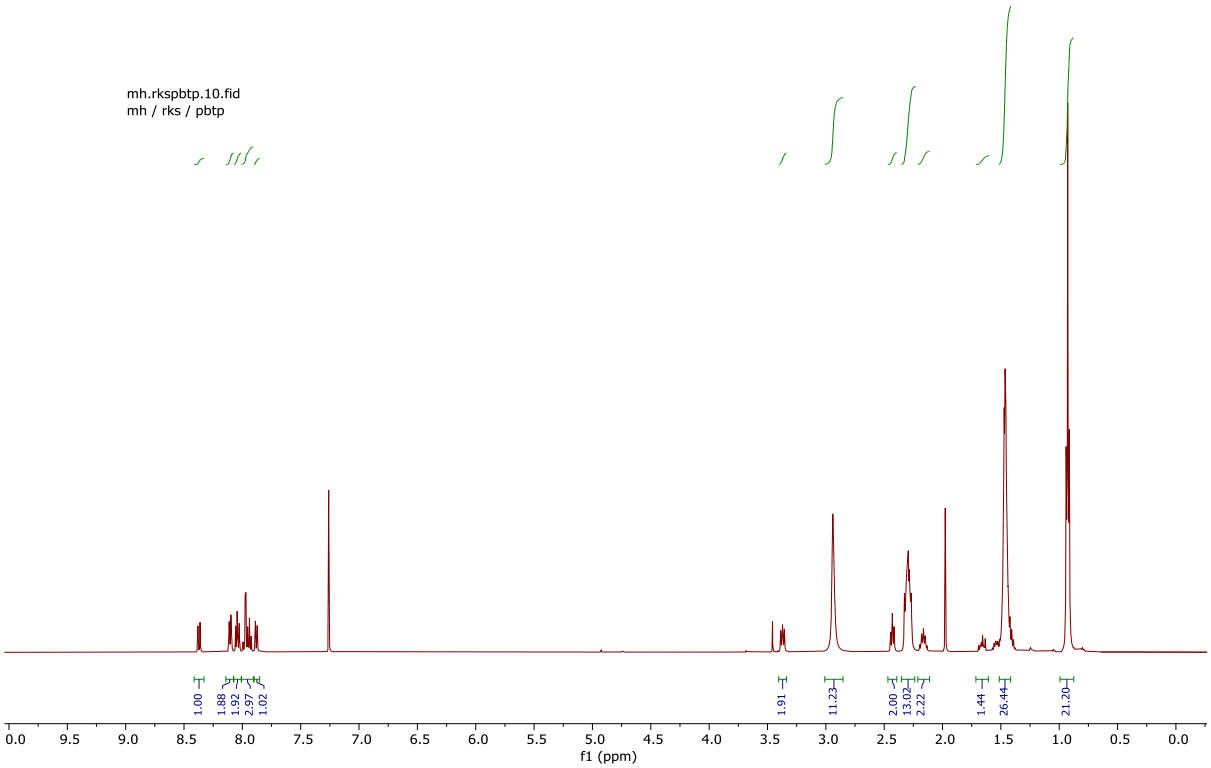

Figure. S6 ^{1}H NMR spectrum ($CDCl_3$, 500 MHz) of PBTBP

^{1}H NMR (500 MHz, Chloroform-*d*) δ 8.38 (d, *J* = 9.2 Hz, 1H), 8.09 (dd, *J* = 7.4, 6.1 Hz, 2H), 8.03 (t, *J* = 8.7 Hz, 2H), 7.96 (d, *J* = 2.5 Hz, 2H), 7.92 (d, *J* = 7.6 Hz, 1H), 7.88 (d, *J* = 7.8 Hz, 1H), 3.41 – 3.33 (m, 2H), 3.27 – 3.22 (m, 8H), 2.46 (t, *J* = 7.4 Hz, 2H), 2.18 (tt, *J* = 10.1, 6.6 Hz, 2H), 1.57 (qd, *J* = 8.1, 7.7, 4.7 Hz, 8H), 1.36 (q, *J* = 7.4 Hz, 8H), 0.93 (t, *J* = 7.4 Hz, 12H).

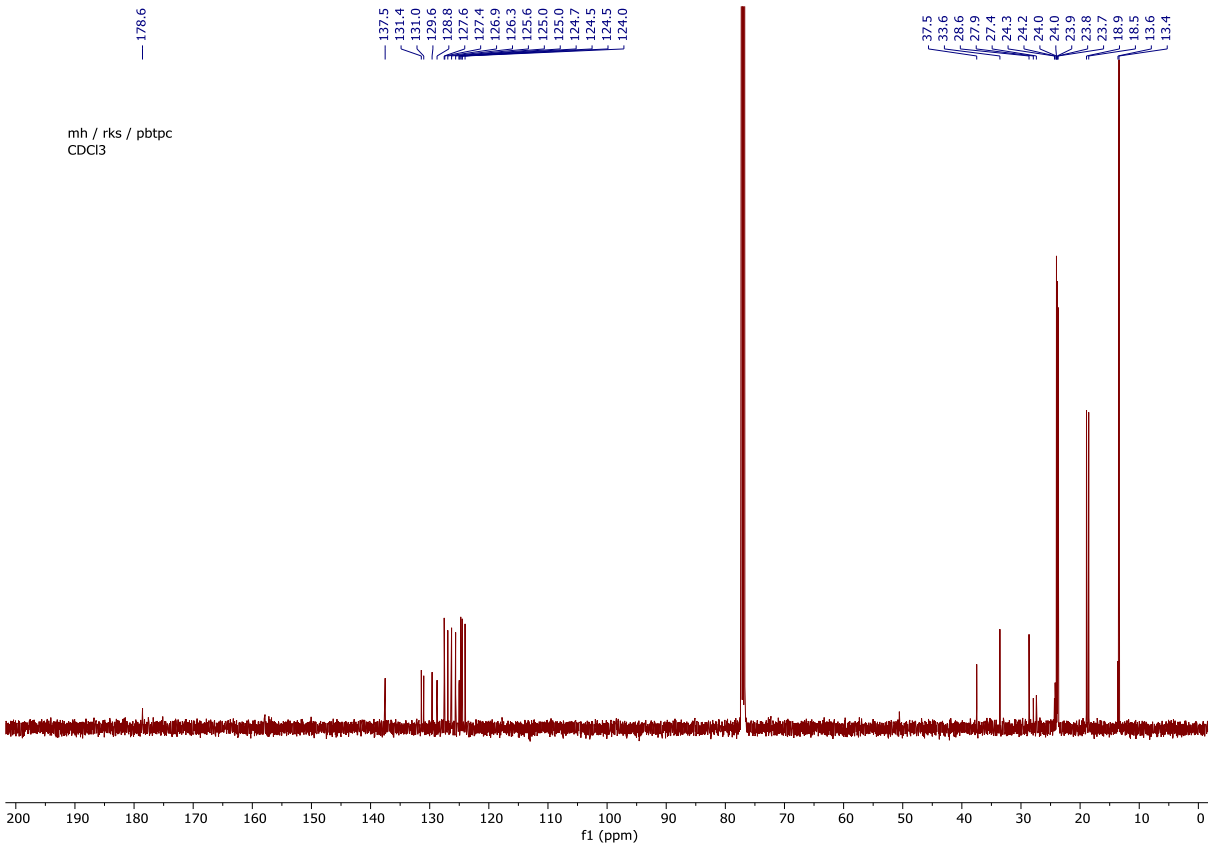

Figure. S7 ^{13}C NMR spectrum ($CDCl_3$, 500 MHz) of PBTBP

^{13}C NMR (126 MHz, $CDCl_3$) δ 178.57, 137.53, 131.42, 131.01, 129.60, 128.76, 127.55, 127.45, 126.94, 126.30, 125.62, 125.04, 125.00, 124.75, 124.54, 124.48, 124.02, 37.49, 33.57, 28.64, 27.91, 27.40, 24.33, 24.22, 24.02, 23.99, 23.87, 23.77, 23.74, 18.92, 18.54, 13.60, 13.42

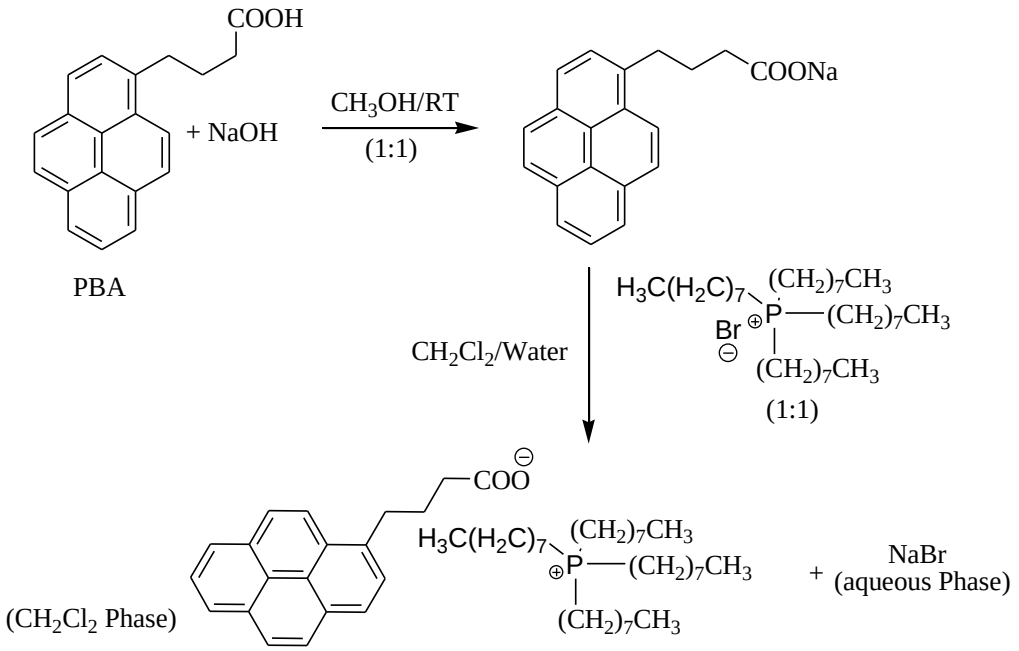

Scheme. S4 Synthetic route for the preparation of PBTOP

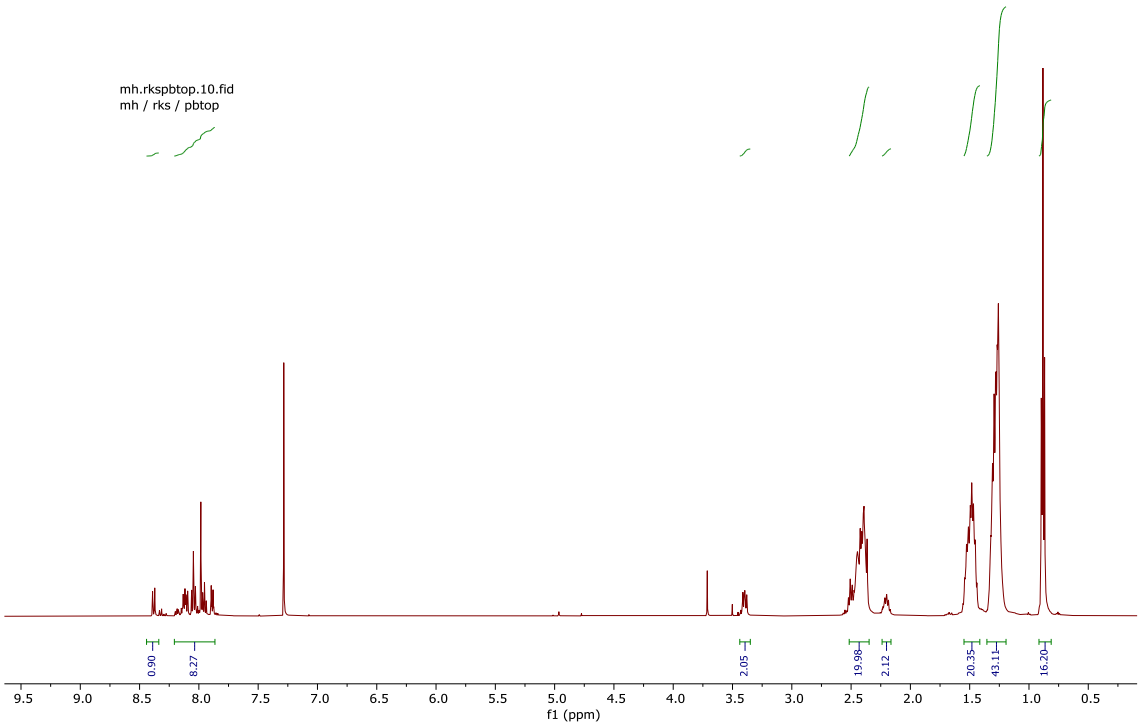

Figure. S8 ^{1}H NMR spectrum ($CDCl_3$, 500 MHz) of PBTOP

^{1}H NMR (500 MHz, Chloroform-*d*) δ 8.38 (d, *J* = 9.2 Hz, 1H), 8.09 (dd, *J* = 7.4, 6.1 Hz, 2H), 8.03 (t, *J* = 8.7 Hz, 2H), 7.96 (d, *J* = 2.5 Hz, 2H), 7.92 (d, *J* = 7.6 Hz, 1H), 7.88 (d, *J* = 7.8 Hz, 1H), 3.41 – 3.33 (m, 2H), 3.27 – 3.22 (m, 8H), 2.46 (t, *J* = 7.4 Hz, 2H), 2.18 (tt, *J* = 10.1, 6.6 Hz, 2H), 1.57 (qd, *J* = 8.1, 7.7, 4.7 Hz, 8H), 1.36 (q, *J* = 7.4 Hz, 8H), 0.93 (t, *J* = 7.4 Hz, 12H).;

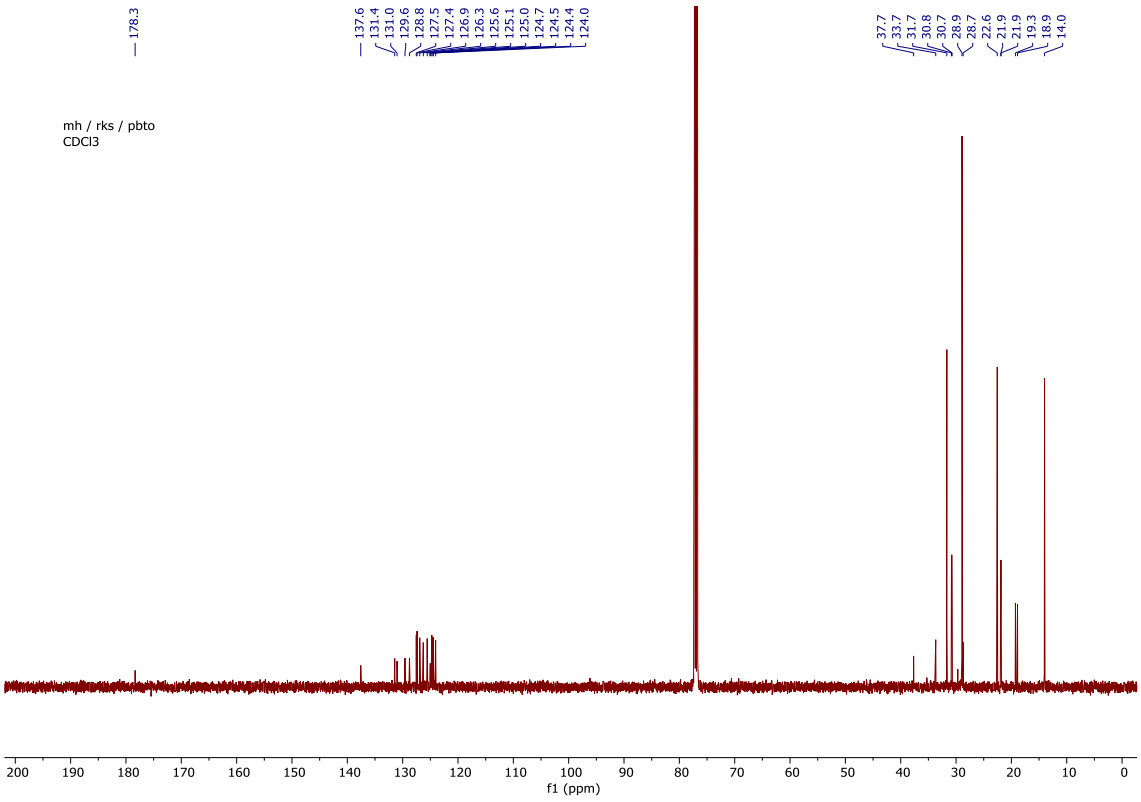

Figure. S9 ^{13}C NMR spectrum ($CDCl_3$, 500 MHz) of PBTOP

^{13}C NMR (126 MHz, $CDCl_3$) δ 178.34, 137.58, 131.43, 131.01, 129.59, 128.77, 127.54, 127.40, 126.92, 126.27, 125.57, 125.06, 125.01, 124.73, 124.51, 124.45, 124.04, 37.67, 33.67, 31.67, 30.78 (d, *J* = 14.5 Hz), 28.92, 28.72, 22.55, 21.89 (d, *J* = 4.9 Hz), 19.27, 18.90, 14.01.

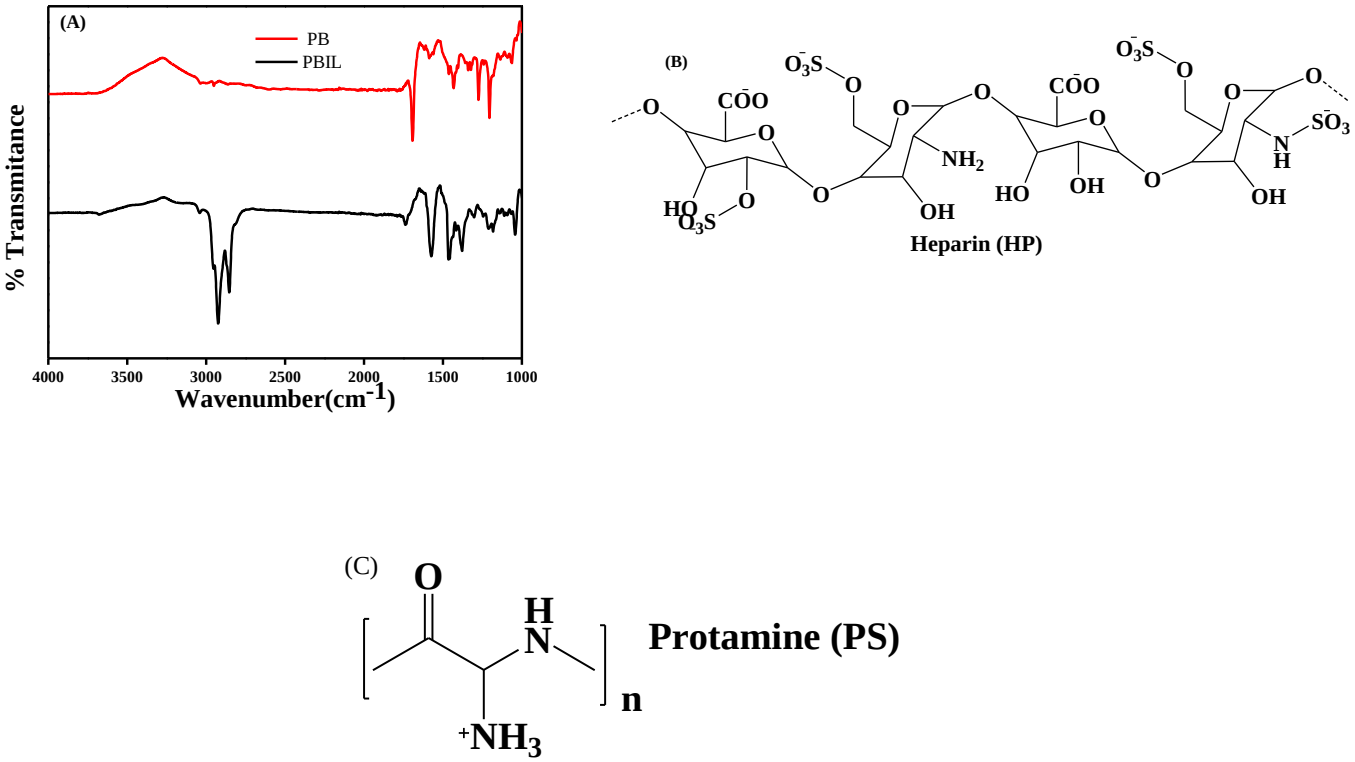

Figure. S10 (A). FTIR spectra of PBIL; (B). Molecular structure heparin; (C). Molecular structure of protamine

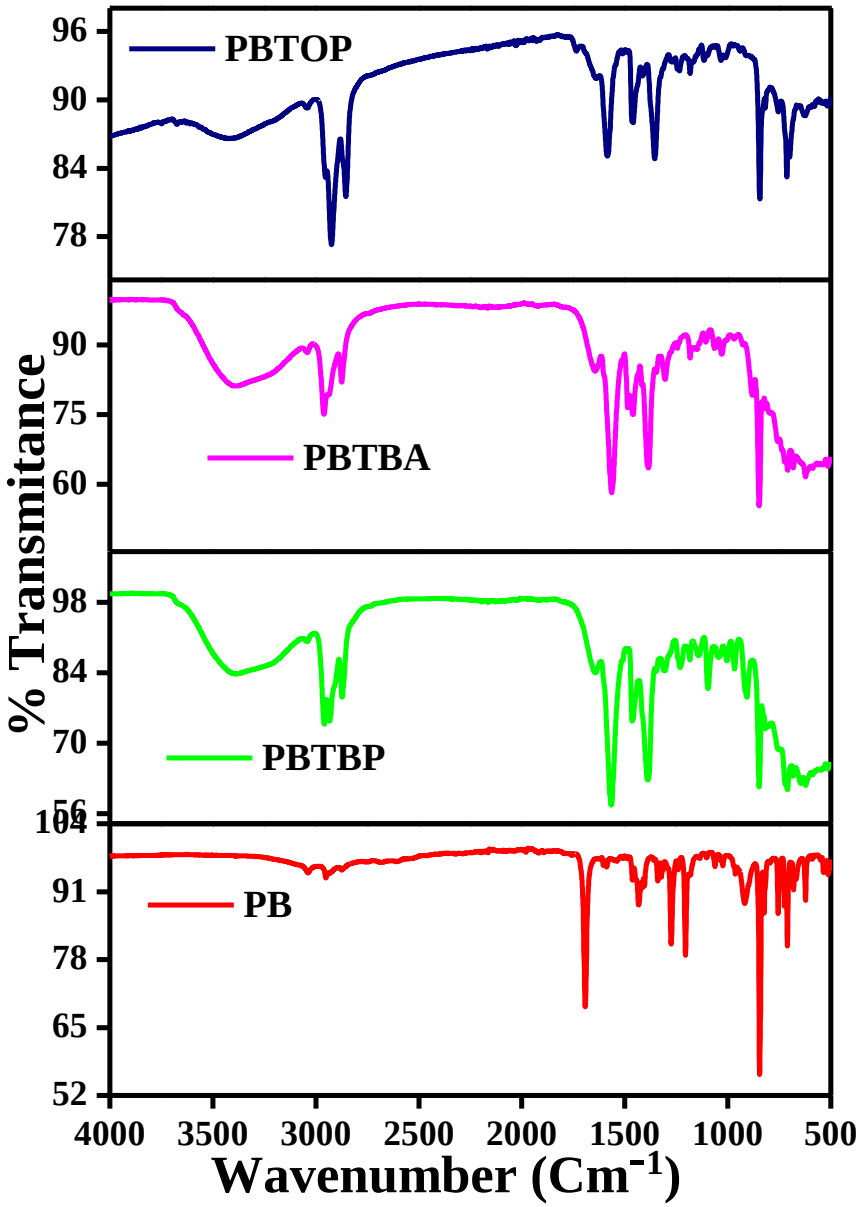

Figure. S11 FTIR spectra of PBTOP, PBTBP, PBTBA, and PB

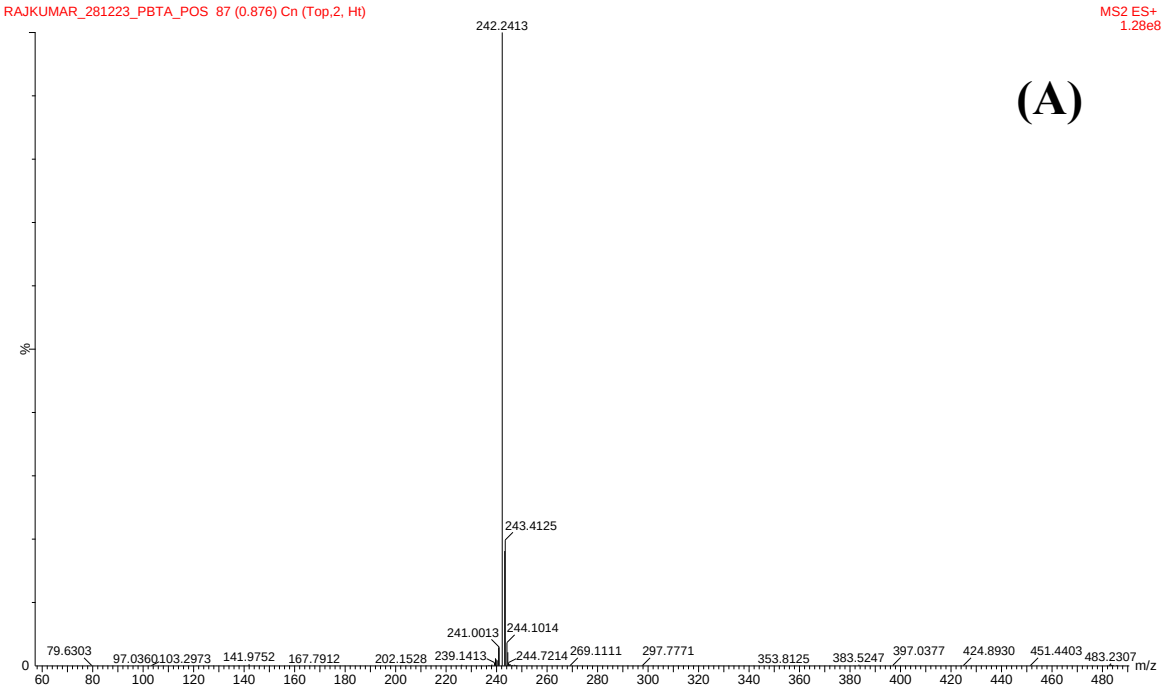
RAJKUMAR_281223_PBTA_POS 87 (0.876) Cn (Top,2, Ht)
MS2 ES+
1.28e8
(A)
242.2413
243.4125
241.0013
244.1014
79.6303
97.0360
103.2973
141.9752
167.7912
202.1528
239.1413
244.7214
269.1111
297.7771
353.8125
383.5247
397.0377
424.8930
451.4403
483.2307
%
0
m/z
60 80 100 120 140 160 180 200 220 240 260 280 300 320 340 360 380 400 420 440 460 480

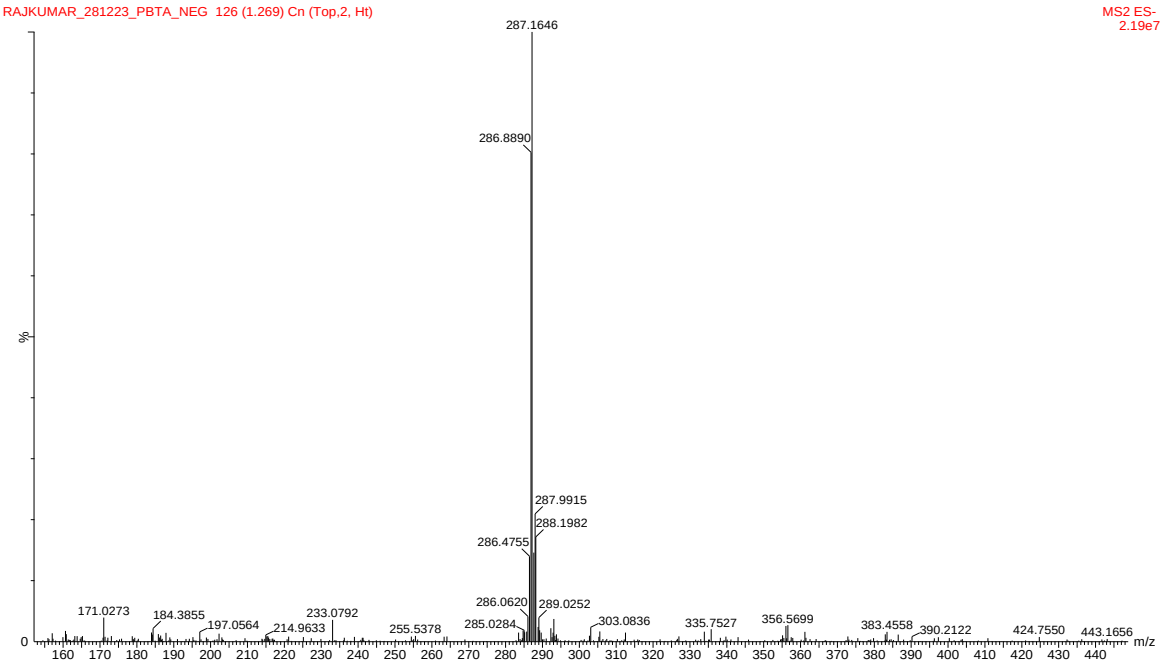
RAJKUMAR_281223_PBTA_NEG 126 (1.269) Cn (Top,2, Ht)
MS2 ES-
2.19e7
287.1646
286.8890
287.9915
288.1982
286.4755
286.0620
289.0252
285.0284
171.0273
184.3855
197.0564
214.9633
233.0792
255.5378
303.0836
335.7527
356.5699
383.4558
390.2122
424.7550
443.1656
%
0
m/z
160 170 180 190 200 210 220 230 240 250 260 270 280 290 300 310 320 330 340 350 360 370 380 390 400 410 420 430 440

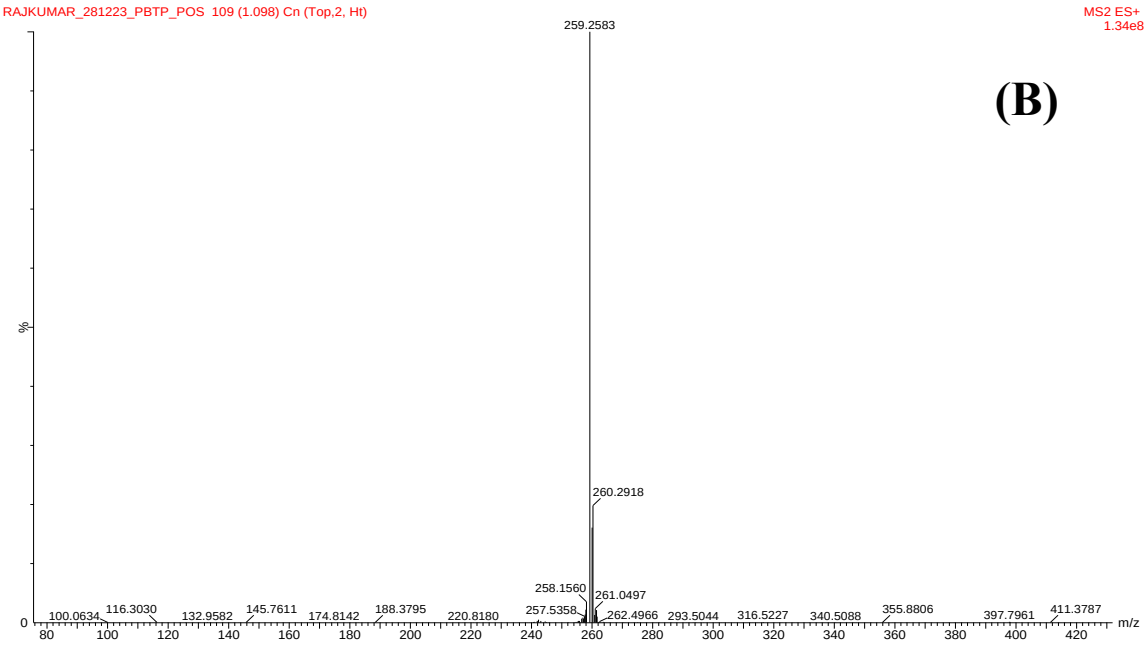
RAJKUMAR_281223_PBTP_POS 109 (1.098) Cn (Top,2, Ht)
MS2 ES+
1.34e8
(B)
259.2583
260.2918
258.1560
261.0497
100.0634
116.3030
132.9582
145.7611
174.8142
188.3795
220.8180
257.5358
262.4966
293.5044
316.5227
340.5088
355.8806
397.7961
411.3787
%
0
m/z
80
100
120
140
160
180
200
220
240
260
280
300
320
340
360
380
400
420

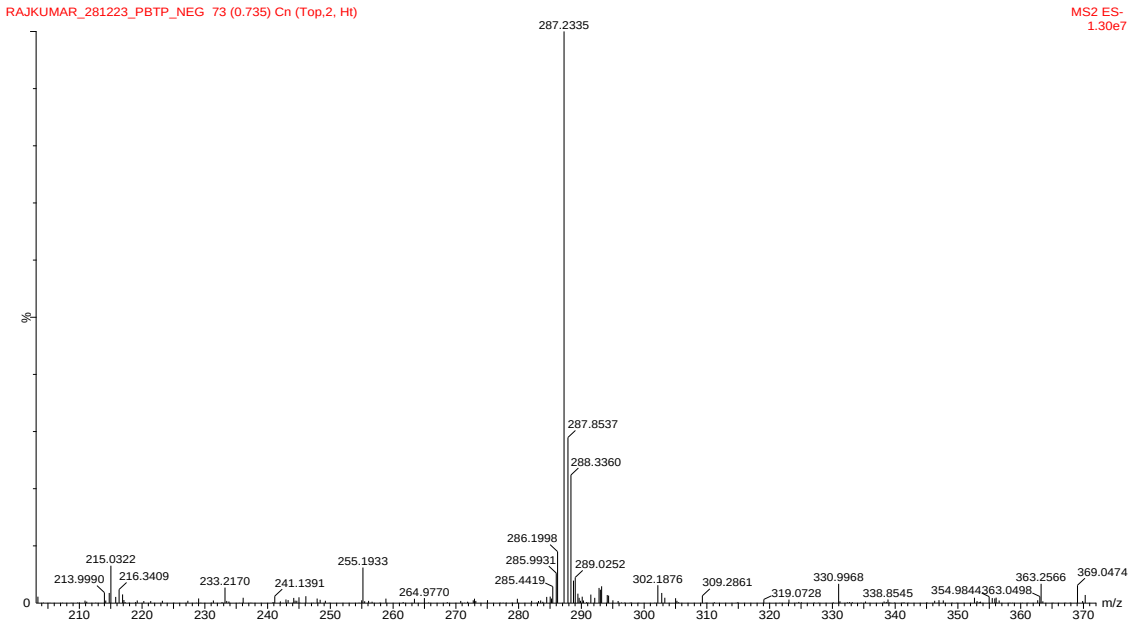
RAJKUMAR_281223_PBTP_NEG 73 (0.735) Cn (Top,2, Ht)
MS2 ES-
1.30e7
287.2335
287.8537
288.3360
286.1998
285.9931
289.0252
215.0322
213.9990
216.3409
233.2170
241.1391
255.1933
264.9770
285.4419
302.1876
309.2861
319.0728
330.9968
338.8545
354.9844
363.0498
363.2566
369.0474
%
0
m/z
210
220
230
240
250
260
270
280
290
300
310
320
330
340
350
360
370

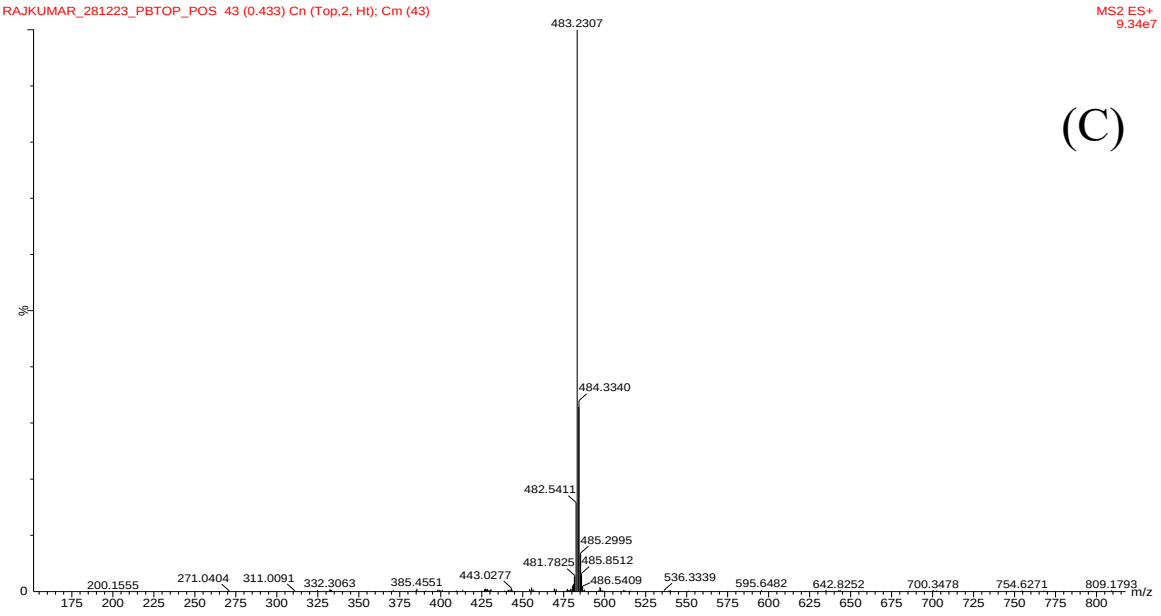
RAJKUMAR_281223_PBTOP_POS 43 (0.433) Cn (Top,2, Ht); Cm (43)
MS2 ES+
9.34e7
(C)
483.2307
484.3340
482.5411
485.2995
485.8512
481.7825
486.5409
200.1555
271.0404
311.0091
332.3063
385.4551
443.0277
536.3339
595.6482
642.8252
700.3478
754.6271
809.1793
%
m/z

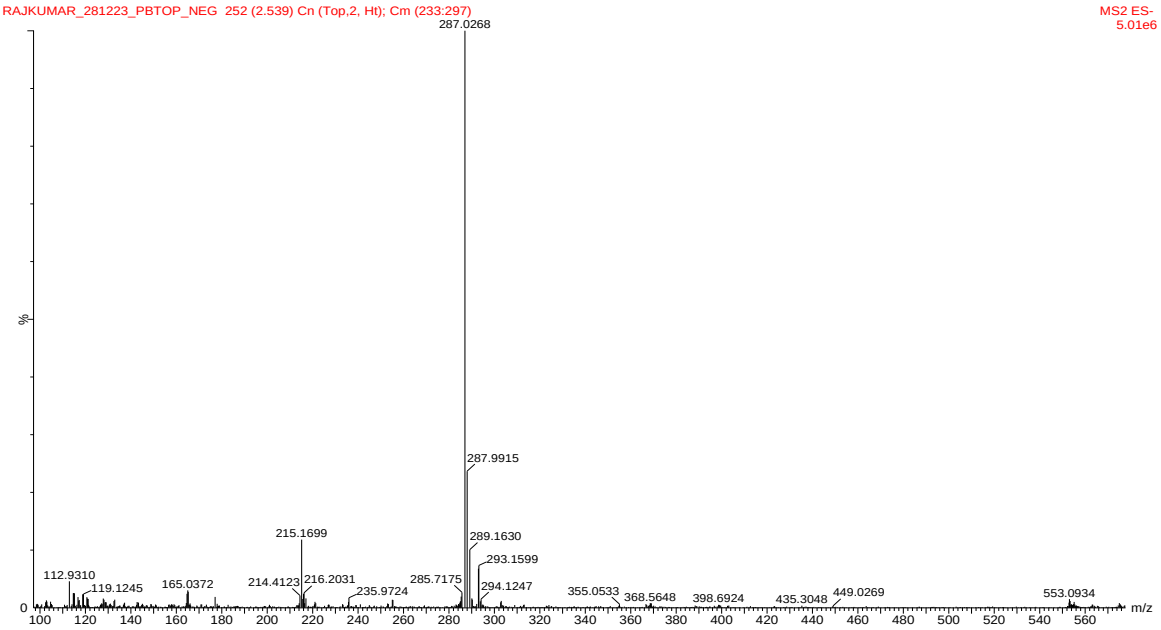
RAJKUMAR_281223_PBTOP_NEG 252 (2.539) Cn (Top,2, Ht); Cm (233:297)
MS2 ES-
5.01e6
287.0268
287.9915
215.1699
289.1630
293.1599
112.9310
119.1245
165.0372
214.4123
216.2031
235.9724
285.7175
294.1247
355.0533
368.5648
398.6924
435.3048
449.0269
553.0934
%
m/z

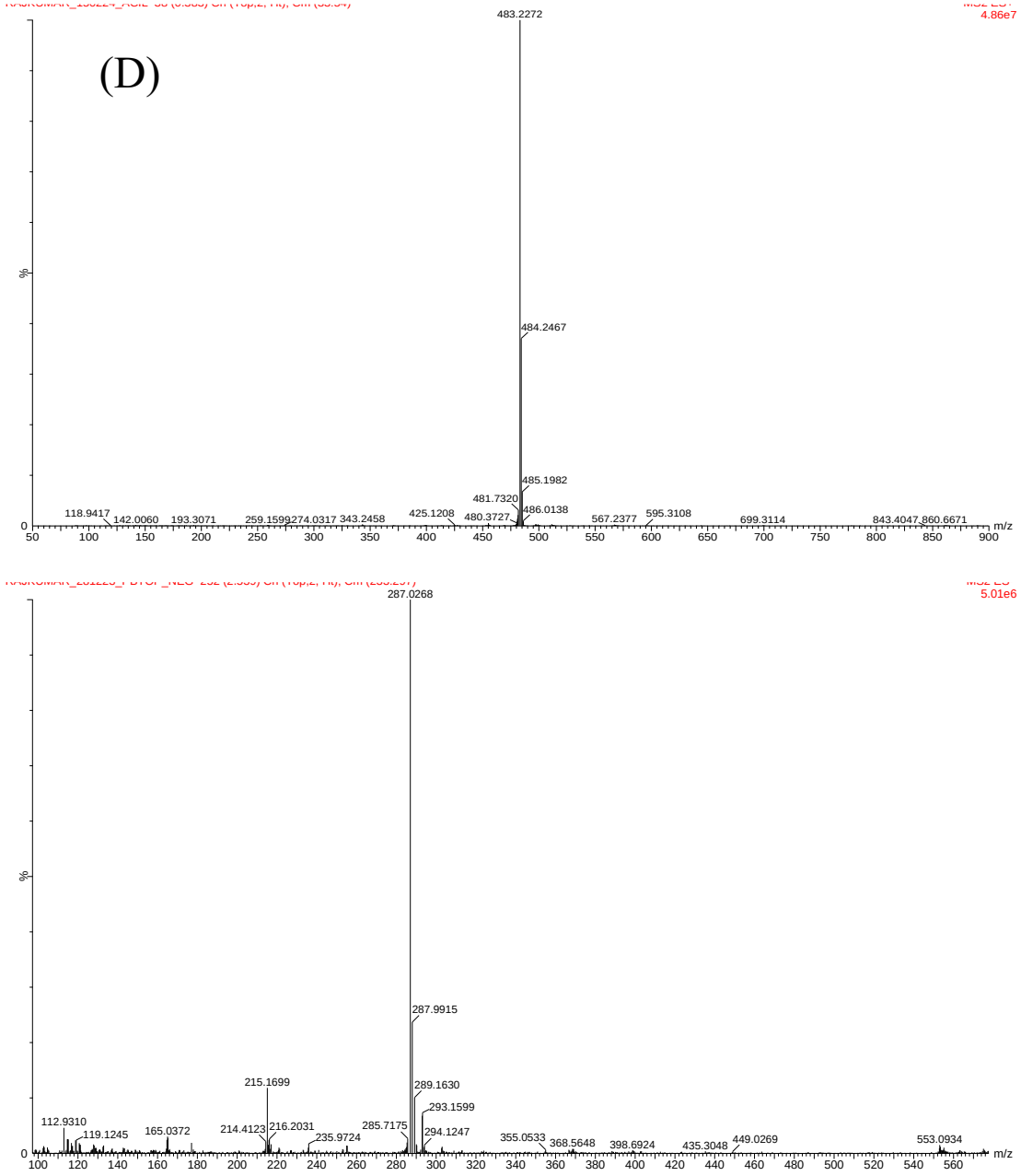

Figure. S12 LCMS data of (A). PBTBA; (B). PBTBP; (C). PBTOP; (D). PBIL

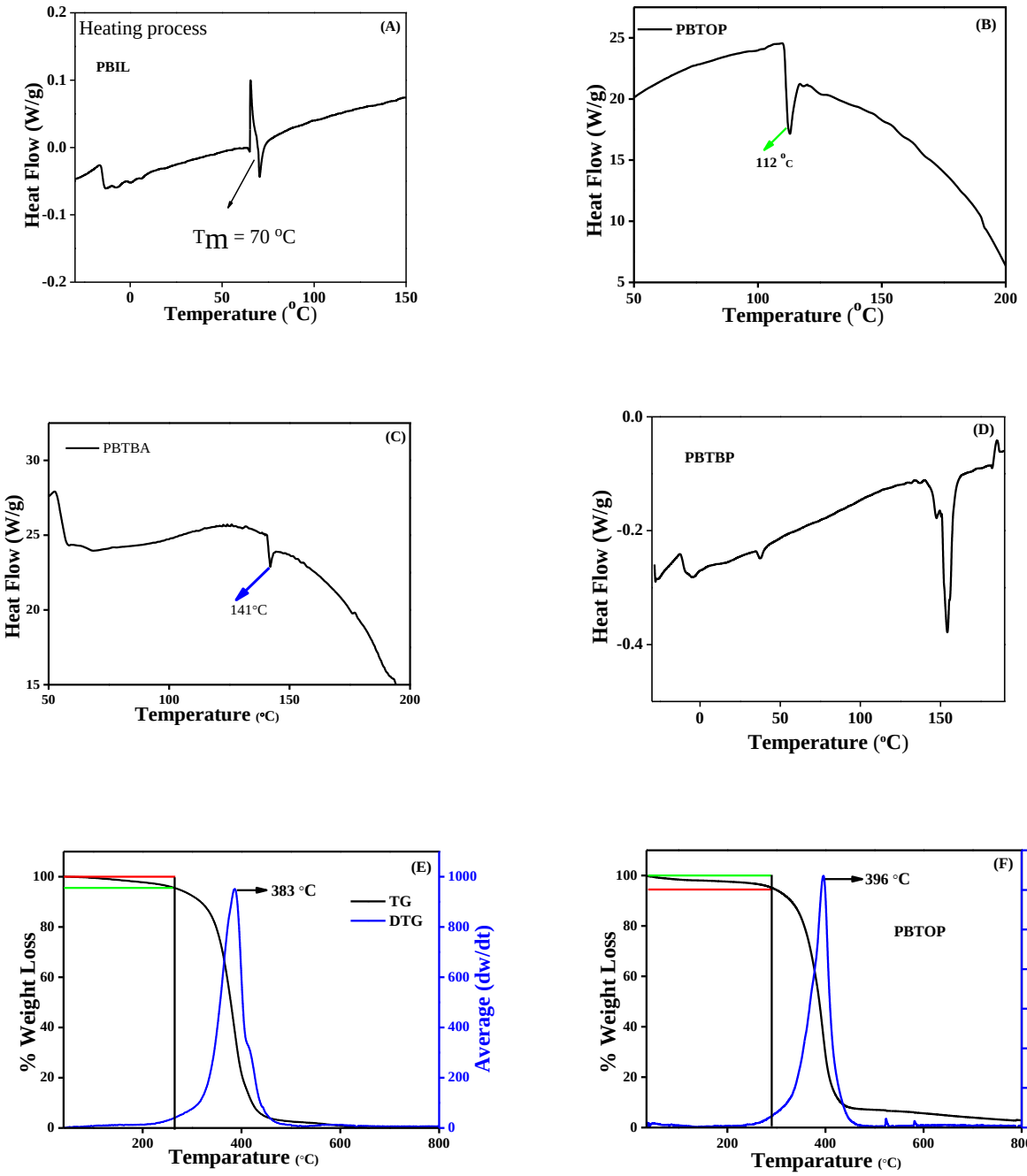

Figure. S13 DSC thermogram under nitrogen atmosphere: (A). PBIL; (B). PBTOP; (C). PBTBA; (D). PBTBP; (E, F). Thermogravimetric analysis of the PBIL and PBTOP

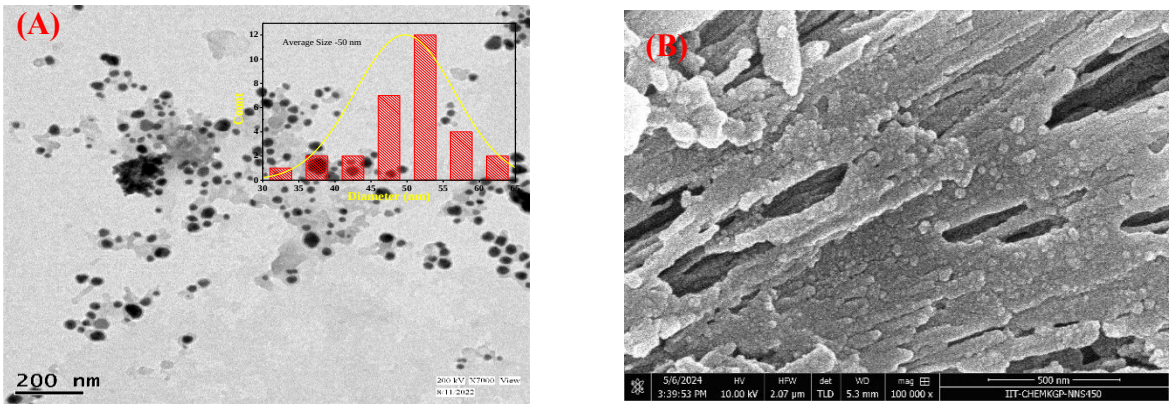

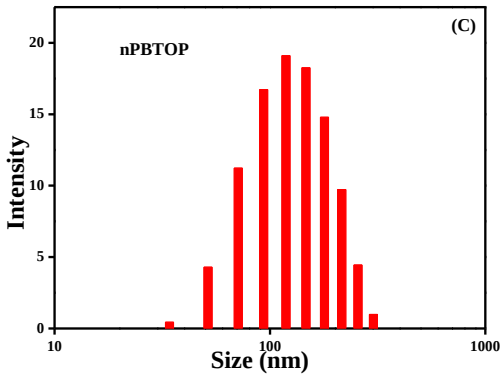

Figure. S14 (A). TEM image of nanoparticles of PBTOP; (B). FESEM image of nanoparticles of PBTOP; (C). DLS spectrum of nanoparticles of PBTOP

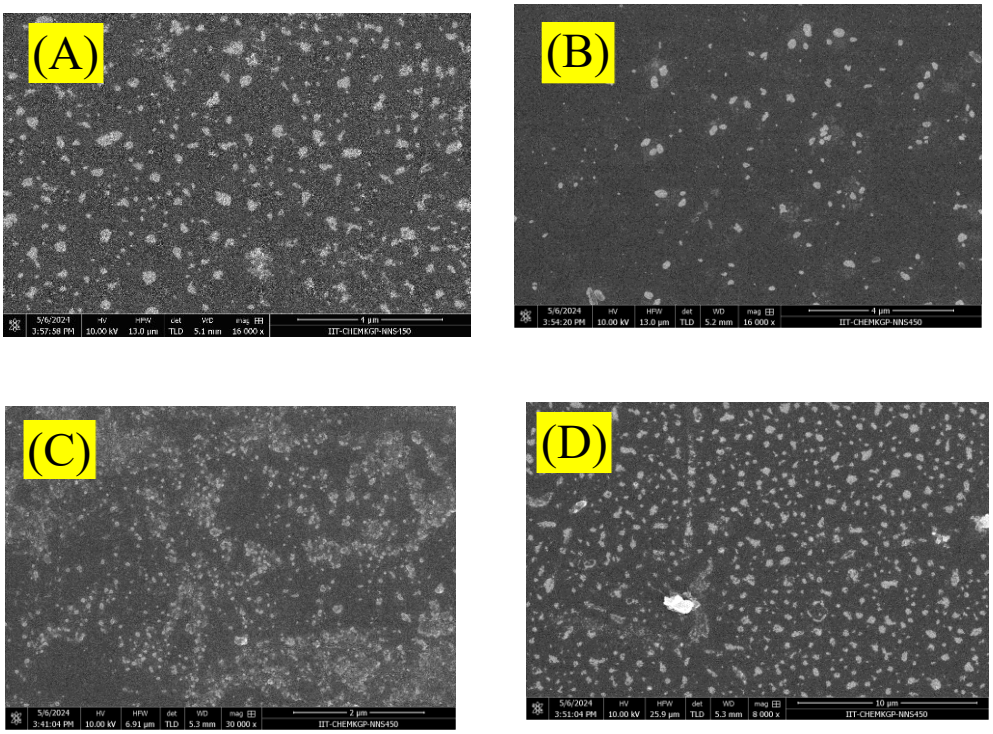

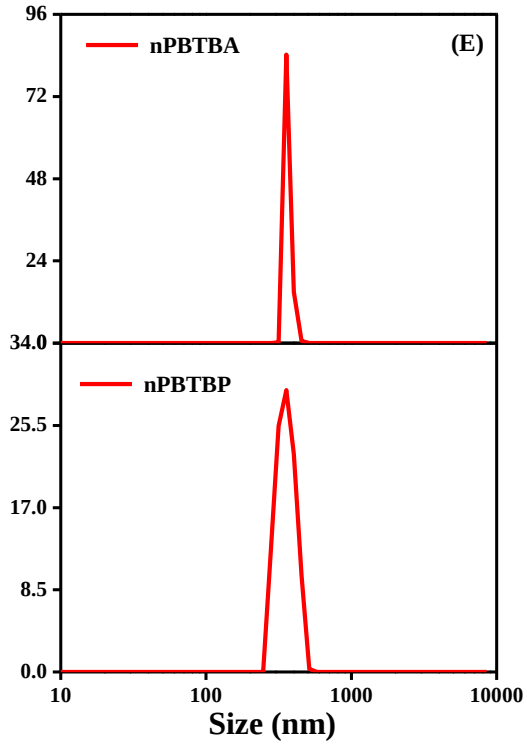

Figure. S15 FESEM image of (A). nPBTBA; (B). nPBTBP; (C). nPBTOP; (D). nPBTOP + Heparin; (E). Hydrodynamic size of nPBTBA and nPBTBP

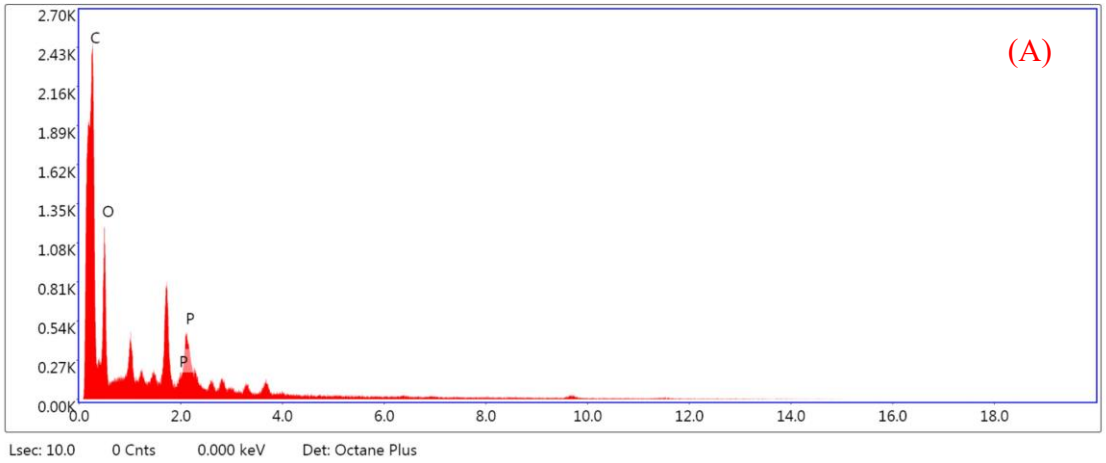

Element	Weight %	Atomic %	Net Int.	Error %
C K	65.74	72.64	4979.04	5.72
O K	31.64	26.24	1601.90	11.70
P K	2.62	1.12	487.18	3.85

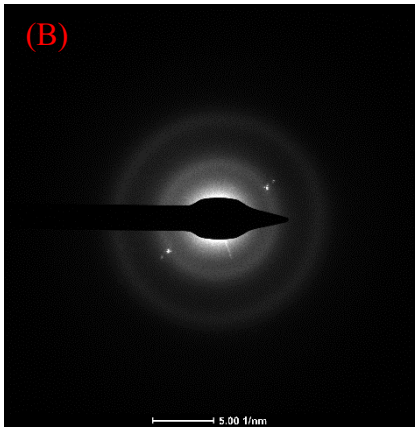

Figure. S16 (A). EDX and (B). SEAD pattern of nPBIL

Table. S1 Absorption maxima, emission maxima*, and quantum yield of nanoGUMBOS in aqueous medium.

*Excited at the absorption maxima

nanoGUMBOS	**λ_{abs} (nm)**	**λ_{em} (nm) (monomer)**	**λ_{em} (nm) (excimer)**	**Φ (%)**	**CIE coordinate**
nPBIL	351	377	480	21.8 ±10	(0.164,0.301)
nPBTOP	351	377	480	21.5 ±10	(0.167,0.296)
nPBTBP	344	377	NA	1.5 ±10	(0.169,0.045)
nPBTBA	344	377	NA	1.6 ±10	(0.17,0.048)

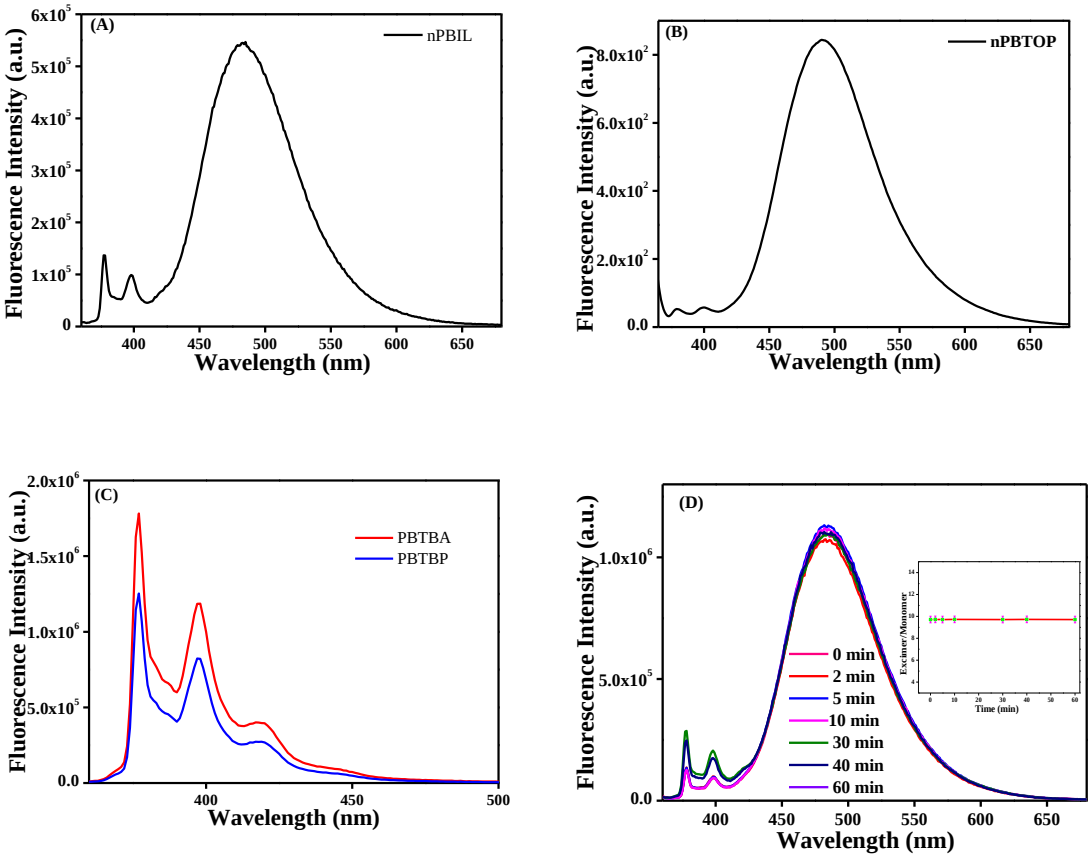

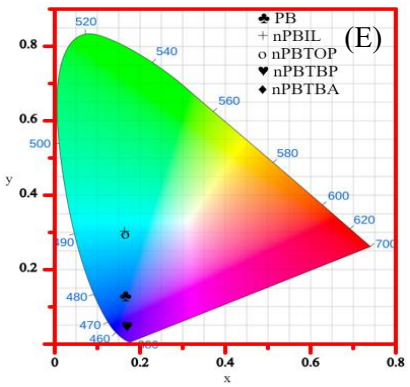

Figure. S17 (A, B, C). Fluorescence spectra of nPBIL (20 µg/mL), nPBTOP, nPBTBA, nPBTBP; (D). Time-Dependent Fluorescence Intensity Change: Assessing the Photostability of nanoGUMBOS (Inset: Plot of intensity at the emission maximum as a function of time); (E). CIE plot of different nanoGUMBOS

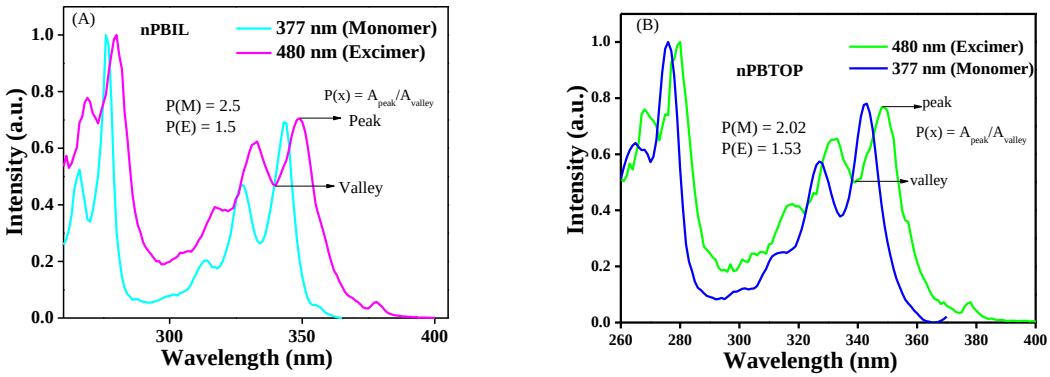

Figure. S18 Fluorescence Excitation spectra of (A). nPBIL and (B). nPBTOP

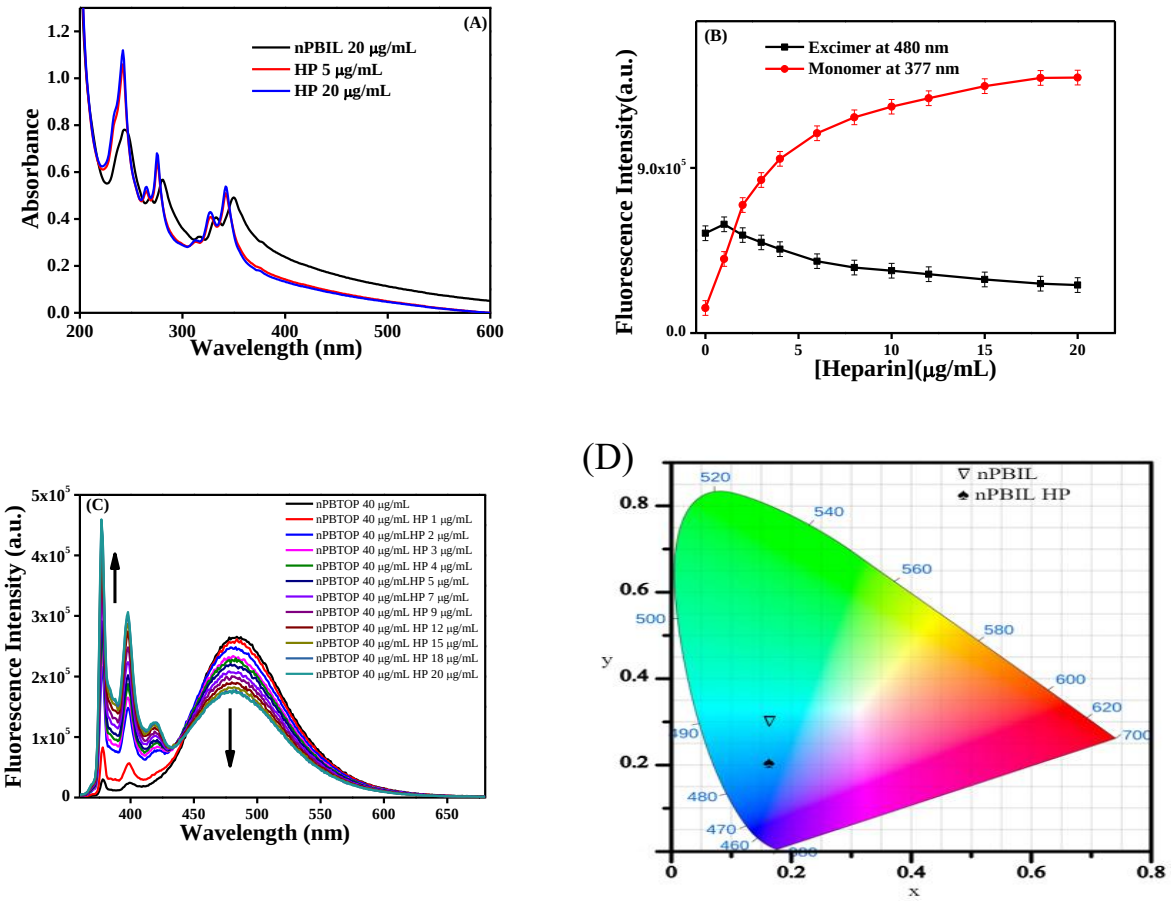

Figure. S19 (A). Absorbance spectra of nPBIL in presence of heparin; (B). Fluorescence intensity change of nPBIL (monomer and excimer region) with the addition of heparin; (C). Fluorescence spectra of nPBTOP with the addition of heparin; (D). CIE plot of nanoGUMBOS in presence of heparin

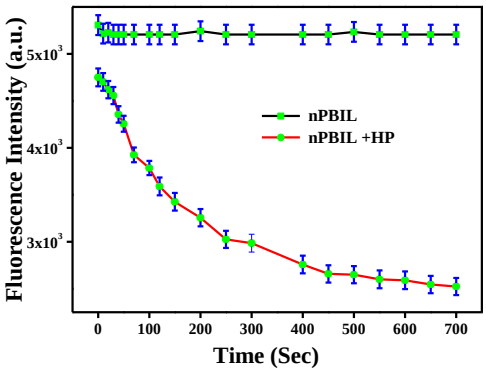

Figure. S20. Time response of nPBIL to heparin in aqueous medium: Change of fluorescence intensity of nPBIL after addition of heparin

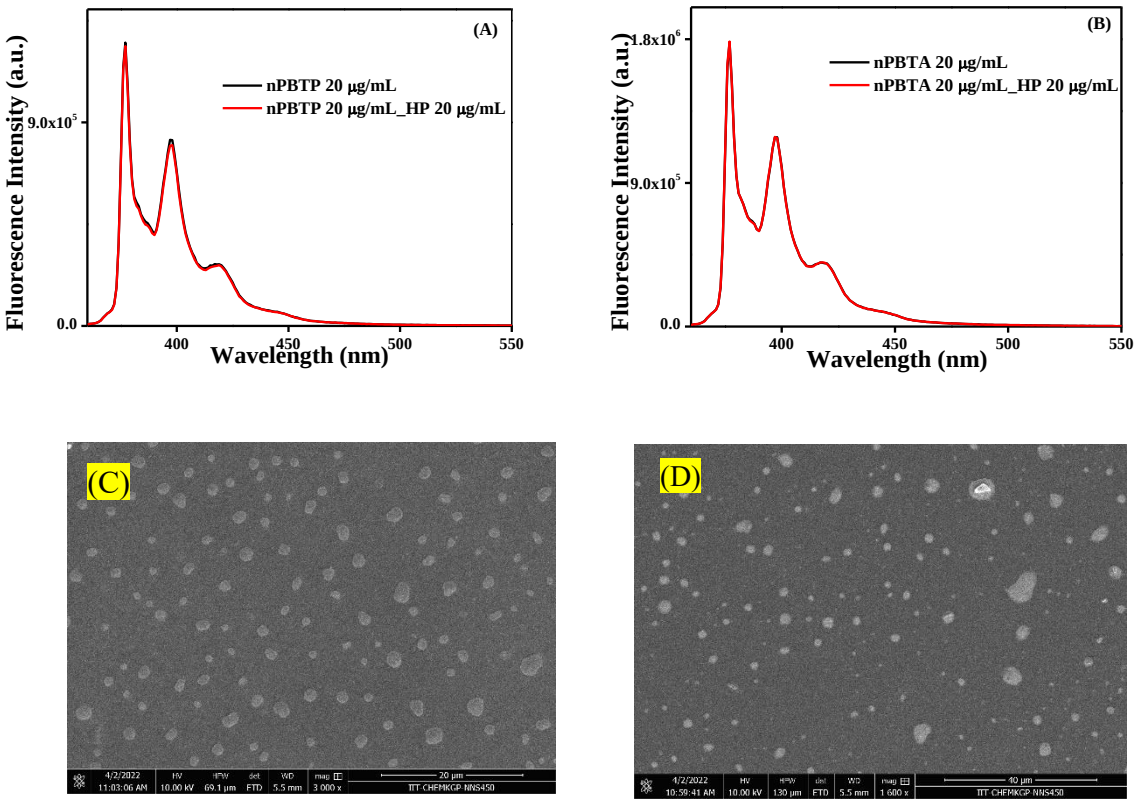

Figure. S21 Fluorescence spectra of (A). nPBTBP and (B). nPBTBA in presence of heparin; (C, D). FESEM image of nPBTBP+ HP and nPBTBA+ HP

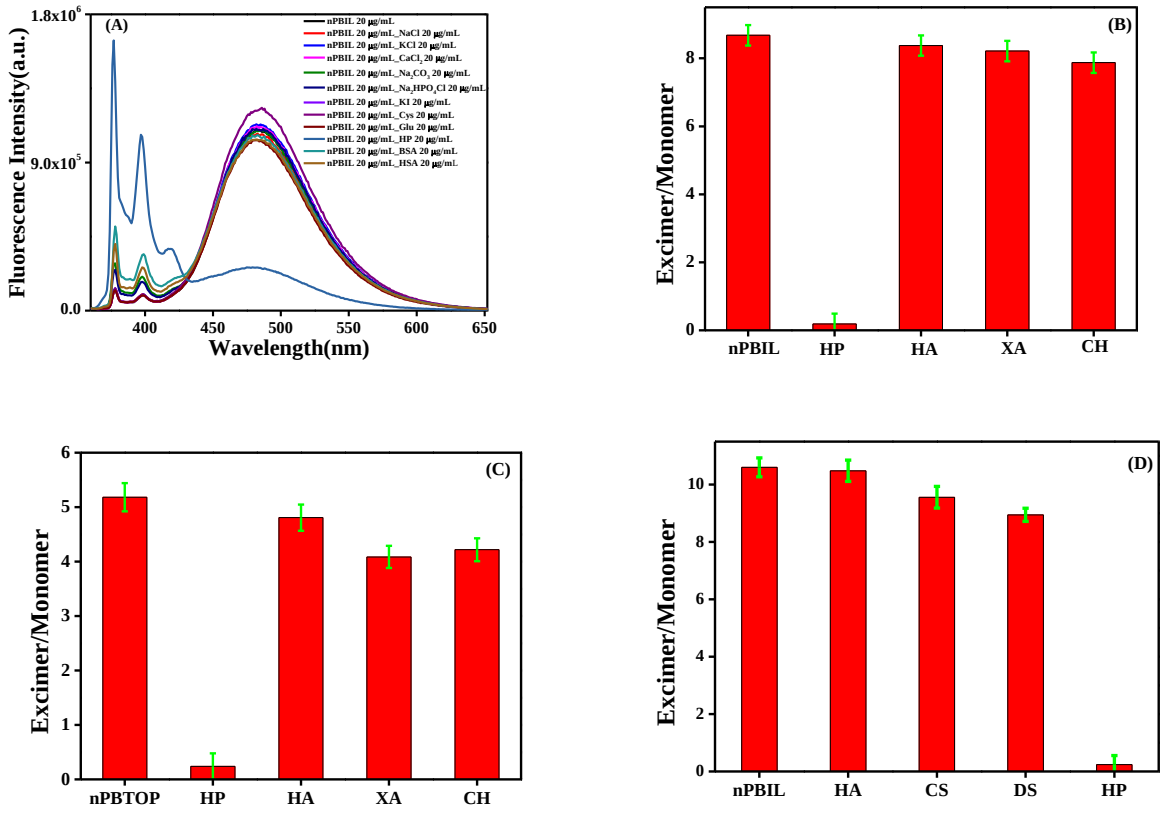

Figure. S22 (A). Fluorescence spectra of nPBIL in the presence of various anions in aqueous medium; (B, C). Bar diagram comparing I_E/I_M values of nPBIL and PBTOP in aqueous solution upon addition of heparin (20 μg/mL), hyaluronic acid (20 μg/mL) (HA), xanthan (20 μg/mL) (XA), and chitosan (20 μg/mL) (CH); (D). Bar diagram comparing I_E/I_M values of nPBIL in aqueous solution upon addition of heparin (HP), hyaluronic acid (HA), chondroitin sulfate (CS), dextran sulfate (DS)

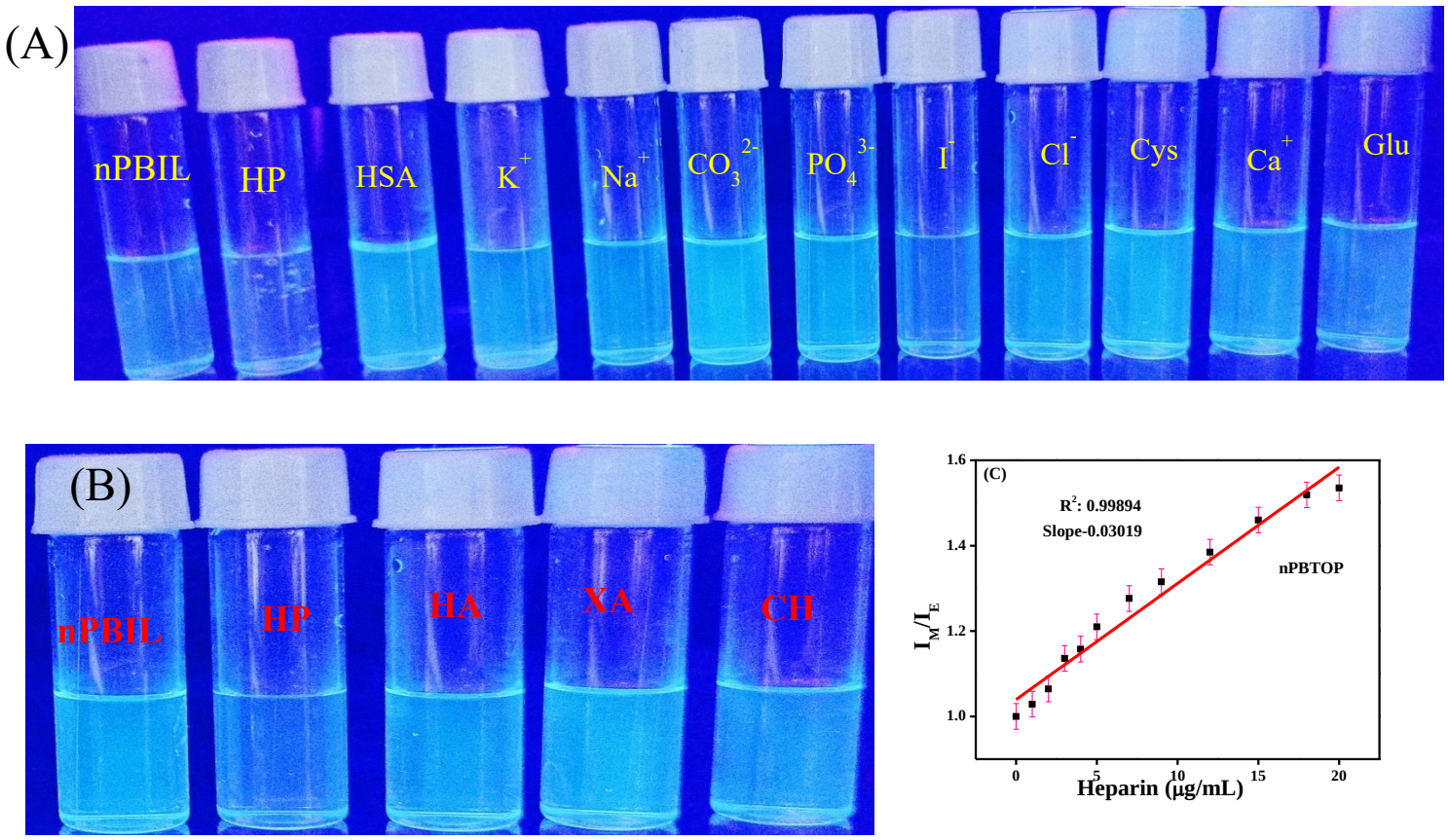

Figure. S23 (A). Picture of nPBIL with the addition various anion and biomolecule including heparin under UV lamp at 365 nm; (B). Picture of nPBIL solution with the addition heparin, hyaluronic acid, xanthan, chitosan under 365 nm UV lamp; (C). Ratio of fluorescence intensity of nPBTOP as a function of heparin

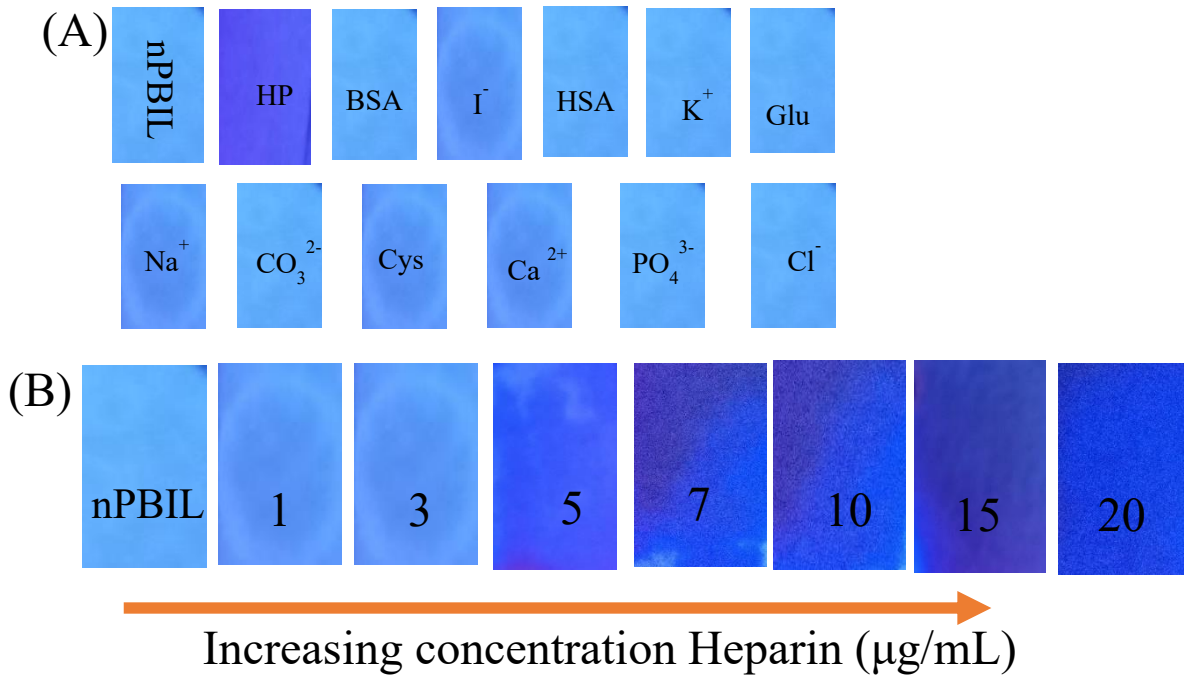

Fig. S24 (A). The colorimetric changes of the paper-strips-based kit for the detection of heparin in an aqueous solution with some biomolecules and anions using the same concentration under a UV lamp at 365 nm; (B). The colorimetric changes of paper kit in the presence of different concentrations of heparin under UV lamp

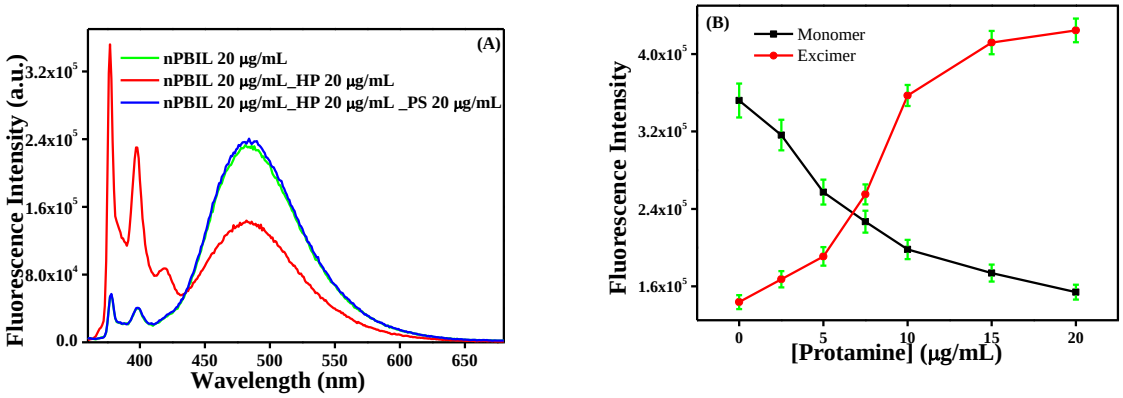

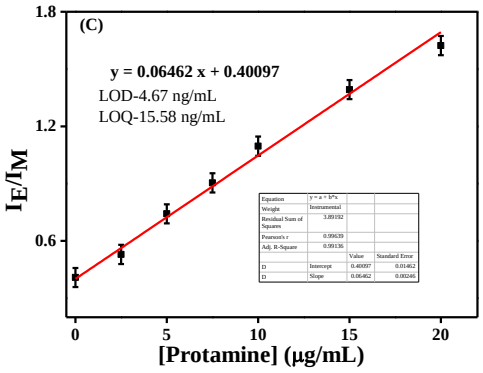

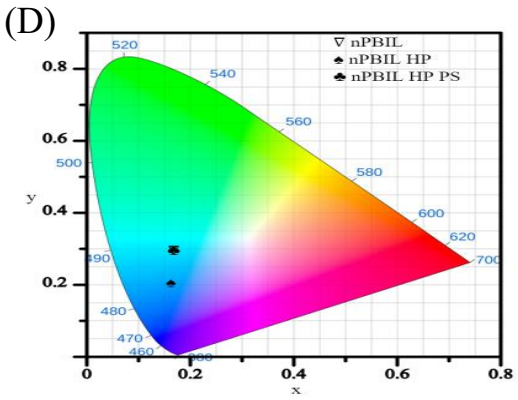

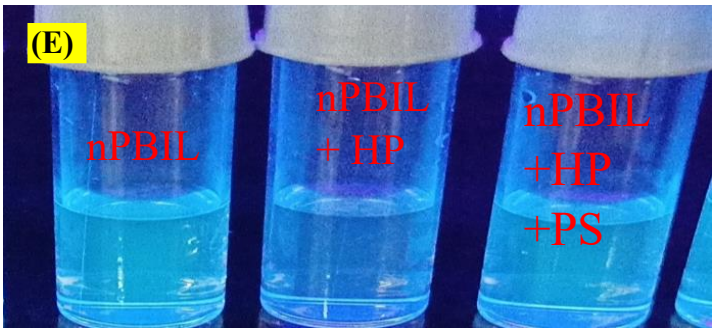

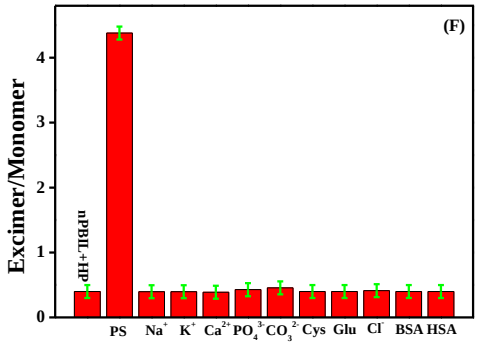

Figure. S25 (A). Fluorescence spectra of nPBIL/Heparin ((20 μg/mL) / (20 μg/mL)) with the addition of protamine sulfate; (B). Fluorescence intensity change of nPBIL-heparin with the addition of protamine sulfate; (C). Ratiometric change fluorescence intensity of nPBIL/Heparin as a function of protamine sulfate; (D). CIE plot of nPBIL, nPBIL+ HP, nPBIL+ HP+ PS; (E). The colorimetric changes of nPBIL in presence of heparin and protamine under UV lamp; (F). Ratiometric response of nPBIL/heparin system in presence of various analytes

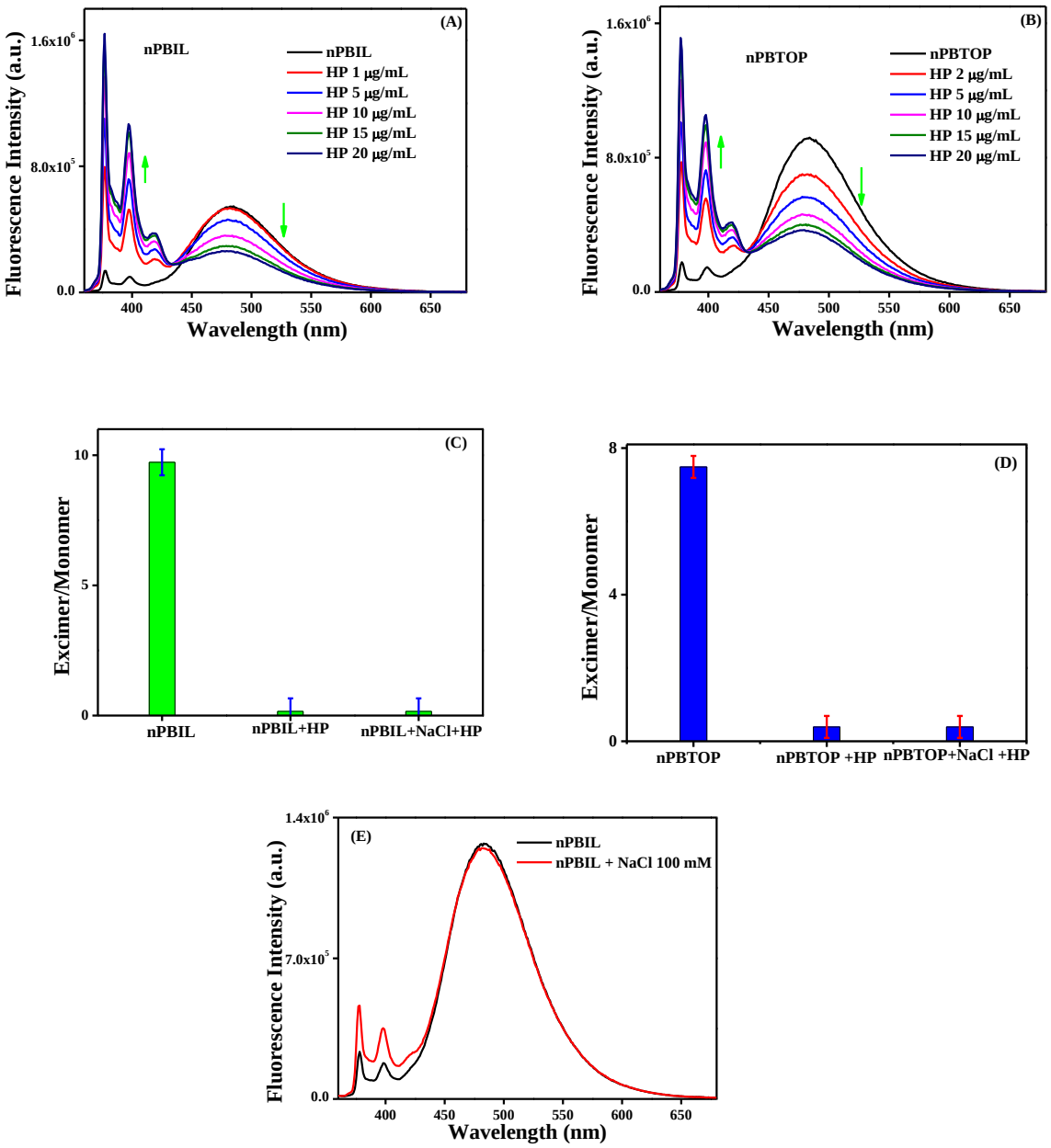

Figure. S26 (A, B). Emission spectral changes of nPBIL and nPBTOP upon addition of heparin in aqueous medium containing 100 mM NaCl; (C, D). Comparative bar diagram of Excimer/monomer of nPBIL and nPBTOP in aqueous medium containing 100 mM NaCl upon addition of heparin; (E). Emission spectra of nPBIL in presence of NaCl

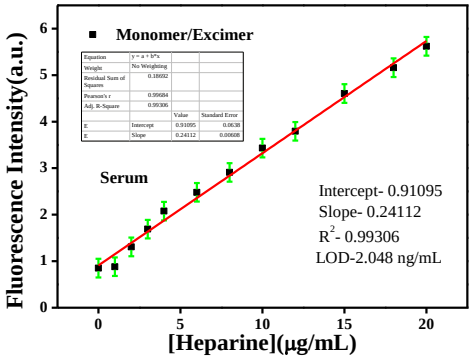

Figure S27. Ratiometric change of fluorescence intensity of nPBIL as a function of heparin in concentration in serum albumin solution

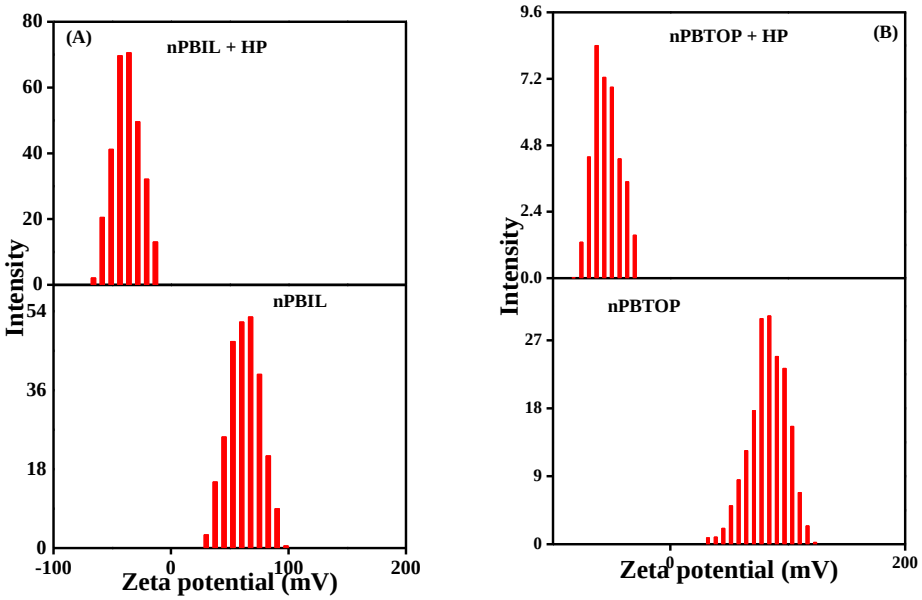

Figure. S28(A) Zeta potential of nPBIL (20 μg/mL) and nPBIL + heparin; (B) Zeta potential of nPBTOP (20 μg/mL) and nPBTOP + heparin

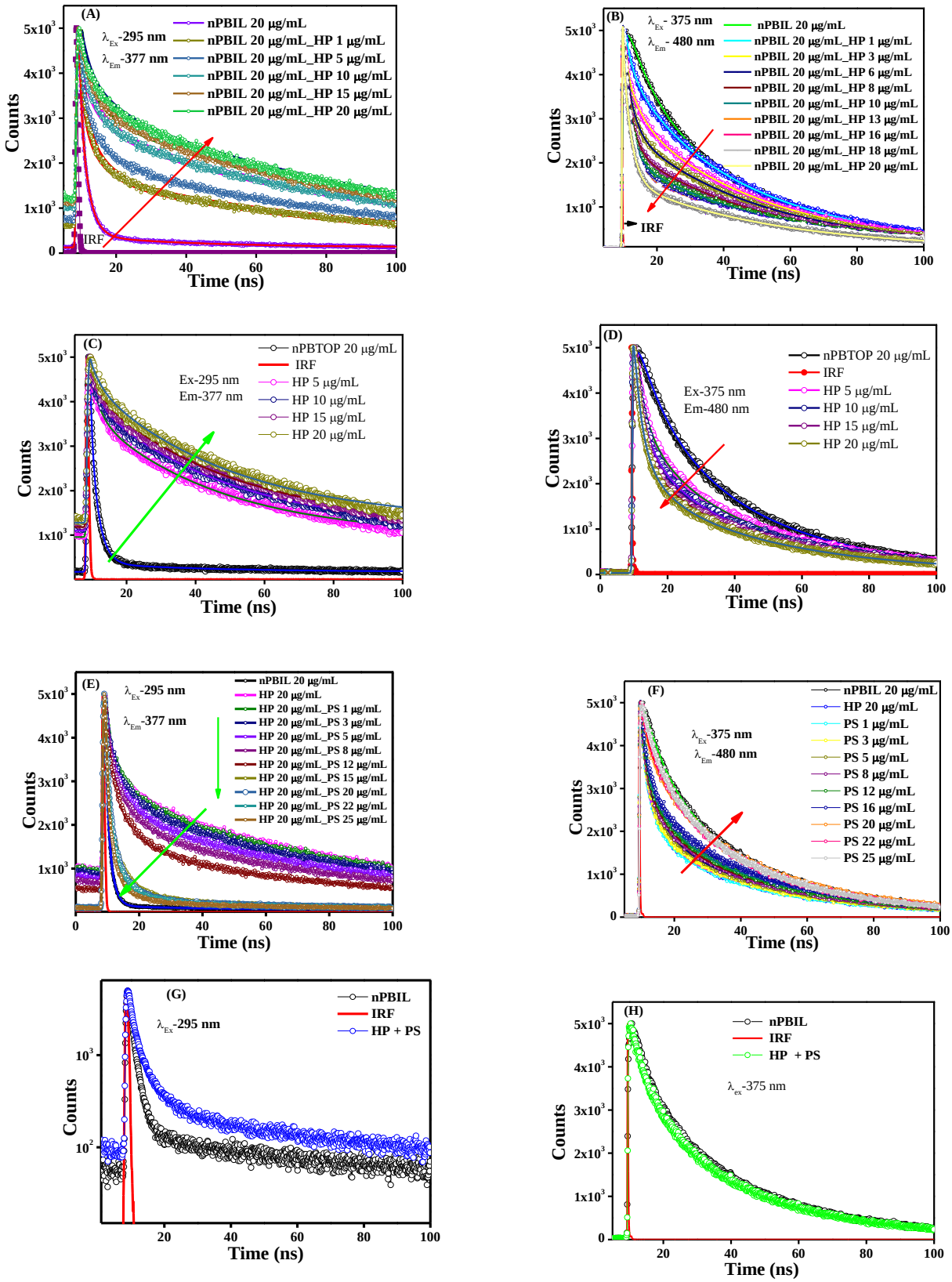

Figure. S29 (A). Lifetime decay of nPBIL in presence of heparin at excitation 295 nm excitation and emission collected 377 nm; (B). Lifetime decay of nPBIL in presence of heparin at excitation 375 nm excitation and emission collected at 480 nm; (C). Lifetime decay of

nPBTOP in presence of heparin at 295 nm excitation and emission collected at 377 nm; (D). Lifetime decay of nPBTOP in presence of heparin at 375 nm excitation and emission collected at 480 nm; (E, G). Lifetime decay of (nPBIL+HP) in presence of protamine, at 295 nm excitation, emission collected at 377 nm; (F, H). Lifetime decay of (nPBIL + HP) with the addition of protamine, at 375 nm excitation, emission collected at 480 nm.

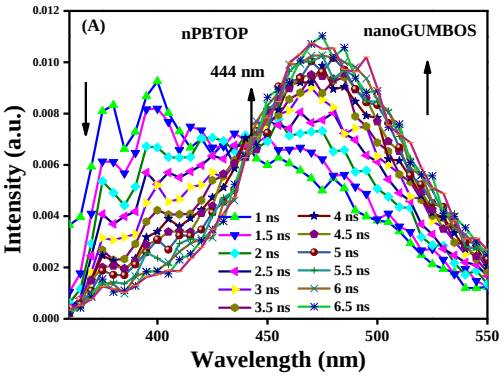

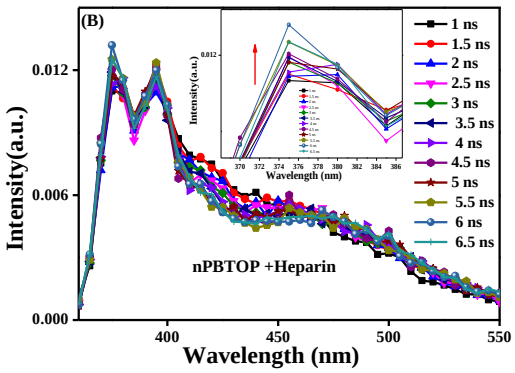

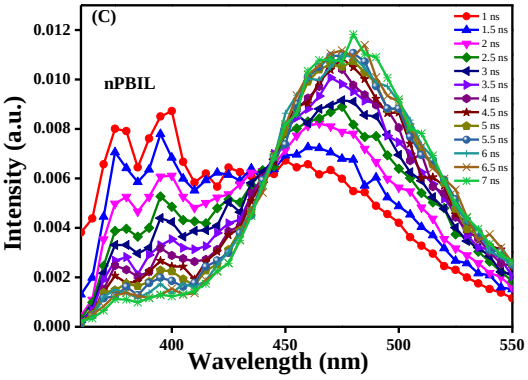

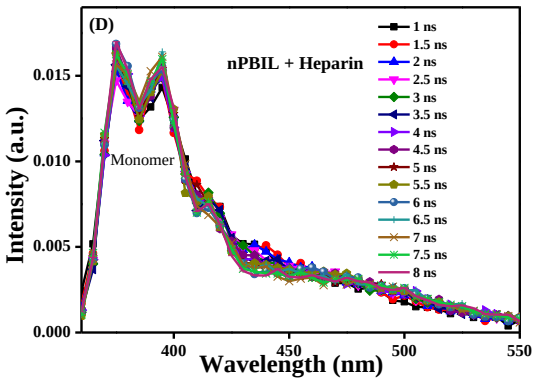

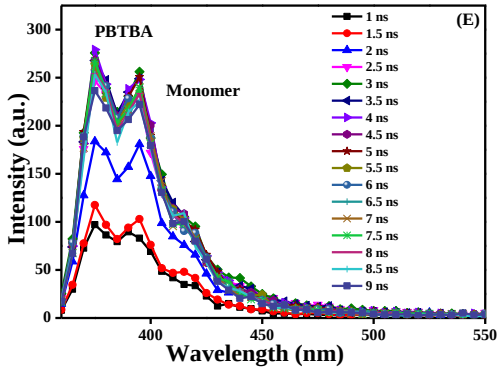

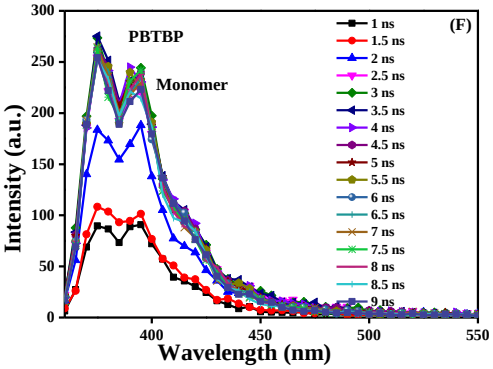

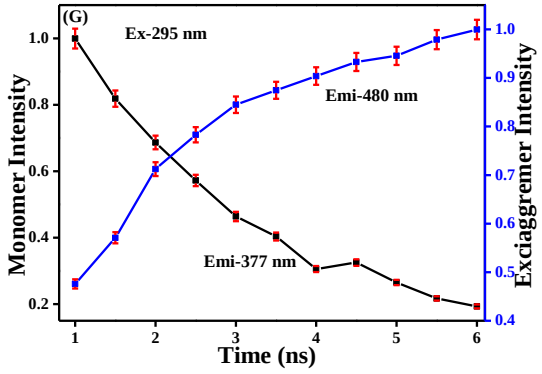

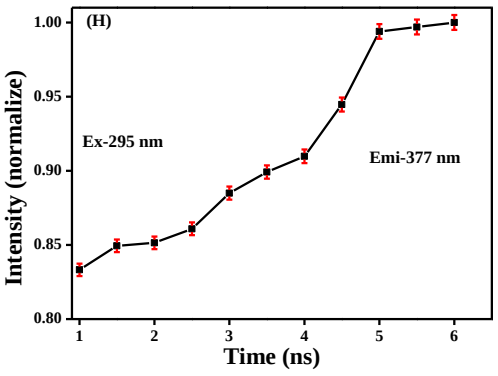

Figure. S30 (A). TRANES spectra of nPBTOP (20 μg/mL), (B) TRANES spectra of nPBTOP (20 μg/mL) in presence of heparin; (C). TRANES spectra of nPBIL, (D). TRANES spectra of nPBIL in presence of heparin (λ_{ex}-295 nm); (E). TRES spectra of PBTBA; (F). TRES spectra of PBTBP; (G). Change of TRANES emission intensity of nanoGUMBOS at the monomer and exciaggremer wavelengths at different times; (H) Change of TRANES emission intensity of nanoGUMBOS in presence of heparin at the monomer wavelength at different times.

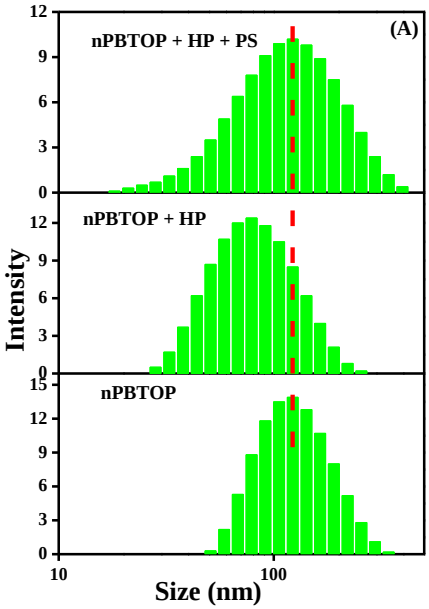

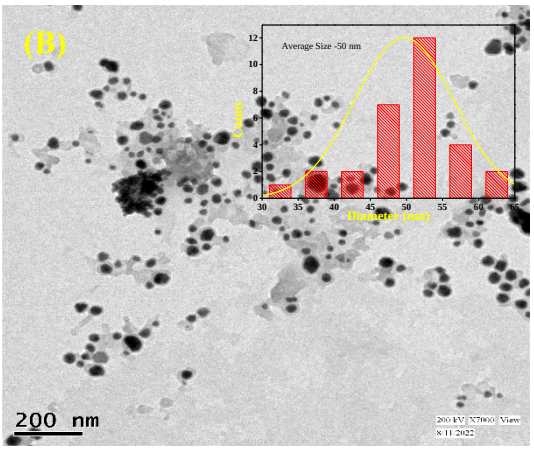

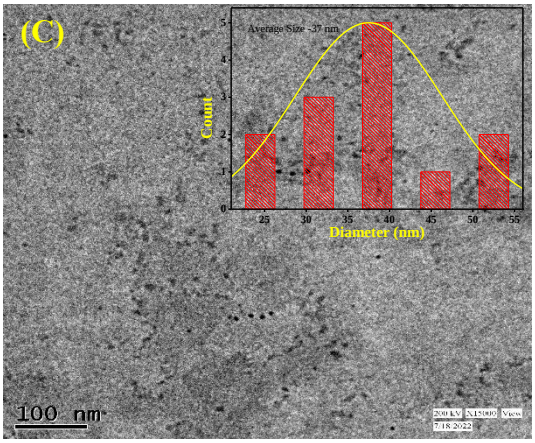

Figure. S31 (A). Hydrodynamic size (diameter) of nPBTOP (20 μg/mL) and nPBTOP + HP, nPBTOP +HP + PS; (B). Representative TEM images of nPBTOP and (C) nPBTOP + HP

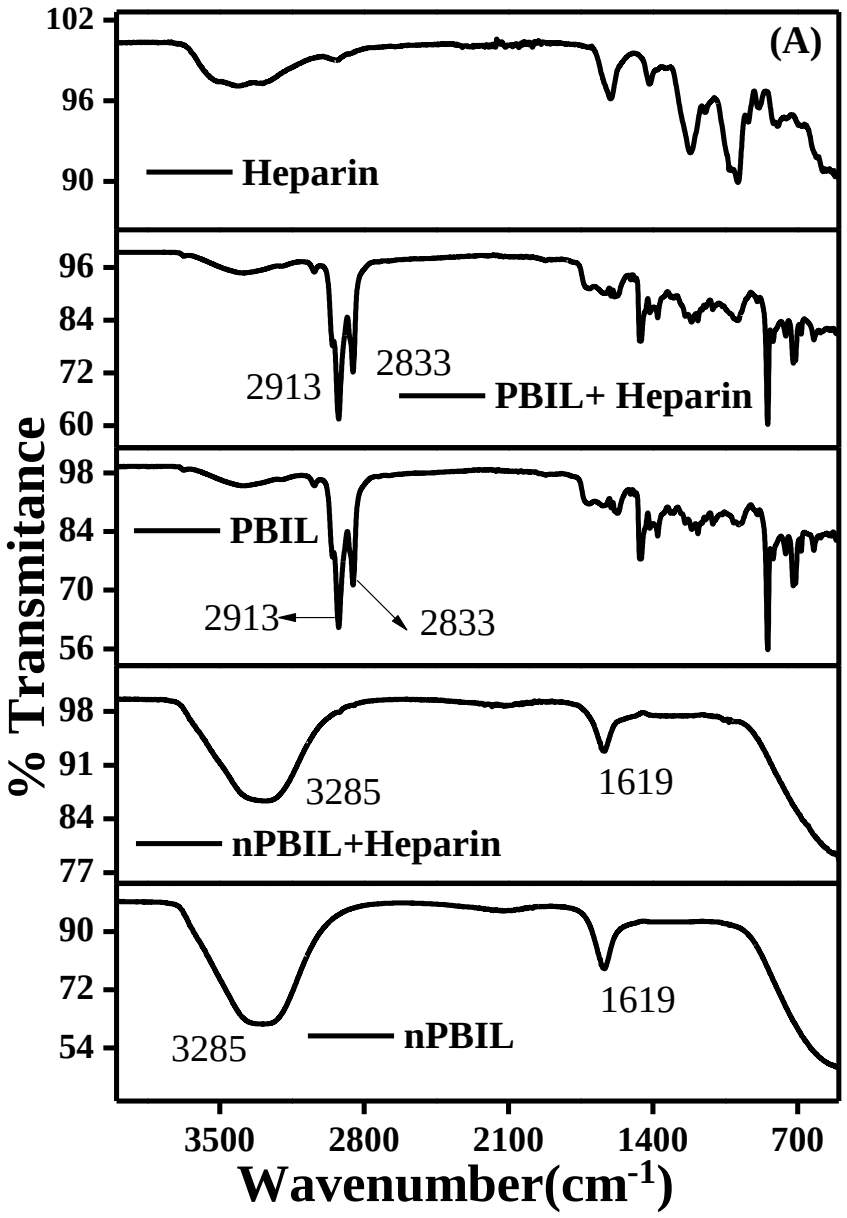
(A)
Heparin
PBIL+ Heparin
2913
2833
PBIL
2913
2833
nPBIL+Heparin
3285
1619
nPBIL
3285
1619
% Transmitance
Wavenumber(cm-1)

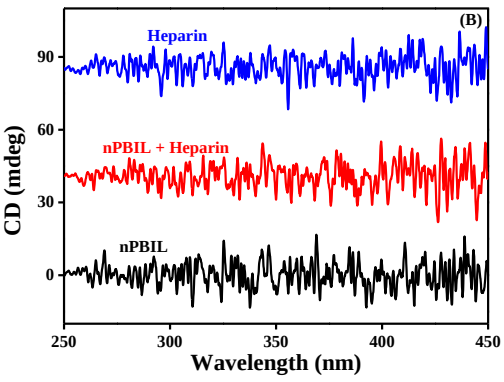
(B)
Heparin
nPBIL + Heparin
nPBIL
CD (mdeg)
Wavelength (nm)

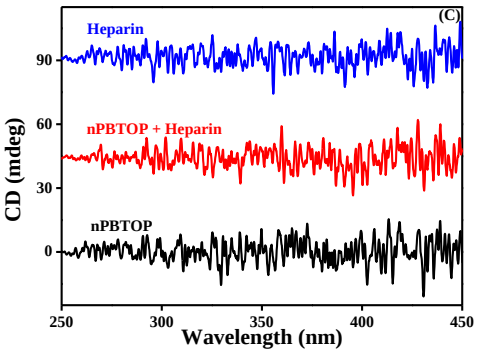
(C)
Heparin
nPBTOP + Heparin
nPBTOP
CD (mdeg)
Wavelength (nm)

Figure. S32 (A). FTIR spectra of PBIL and nPBIL in the absence and presence of heparin; (B). CD spectra of nPBIL (20 µg/mL) in presence of heparin in aqueous medium; (C). CD spectra of nPBTOP (20 µg/mL) in presence of heparin in aqueous medium.

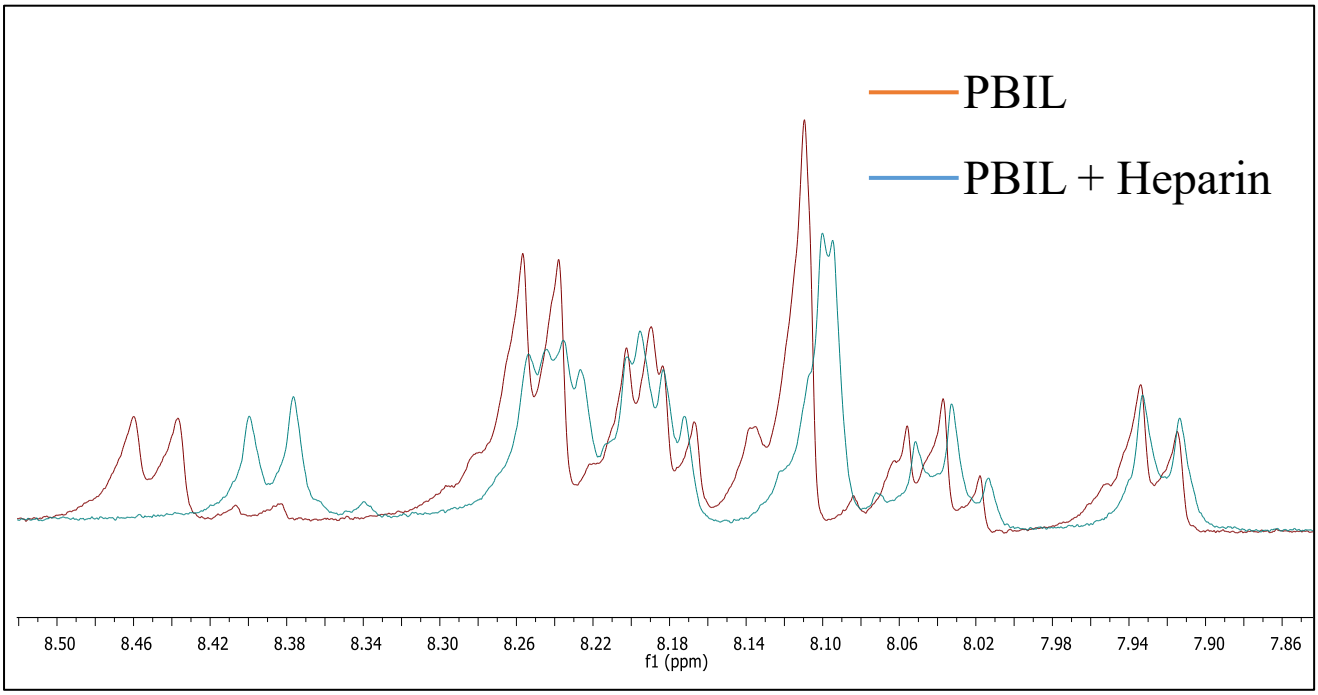

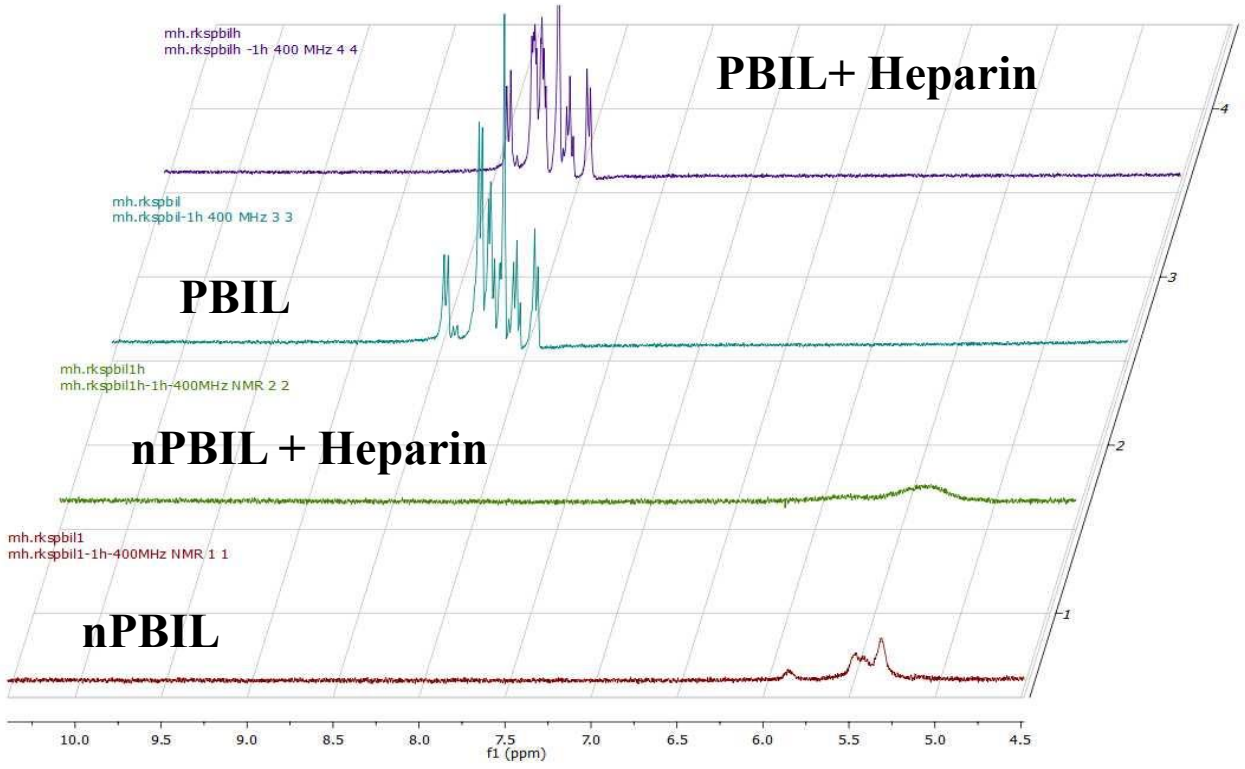

Figure. S33 ^{1}H NMR of aromatic proton of PBIL and nPBIL in the absence and presence of heparin (in DMSO-d6)

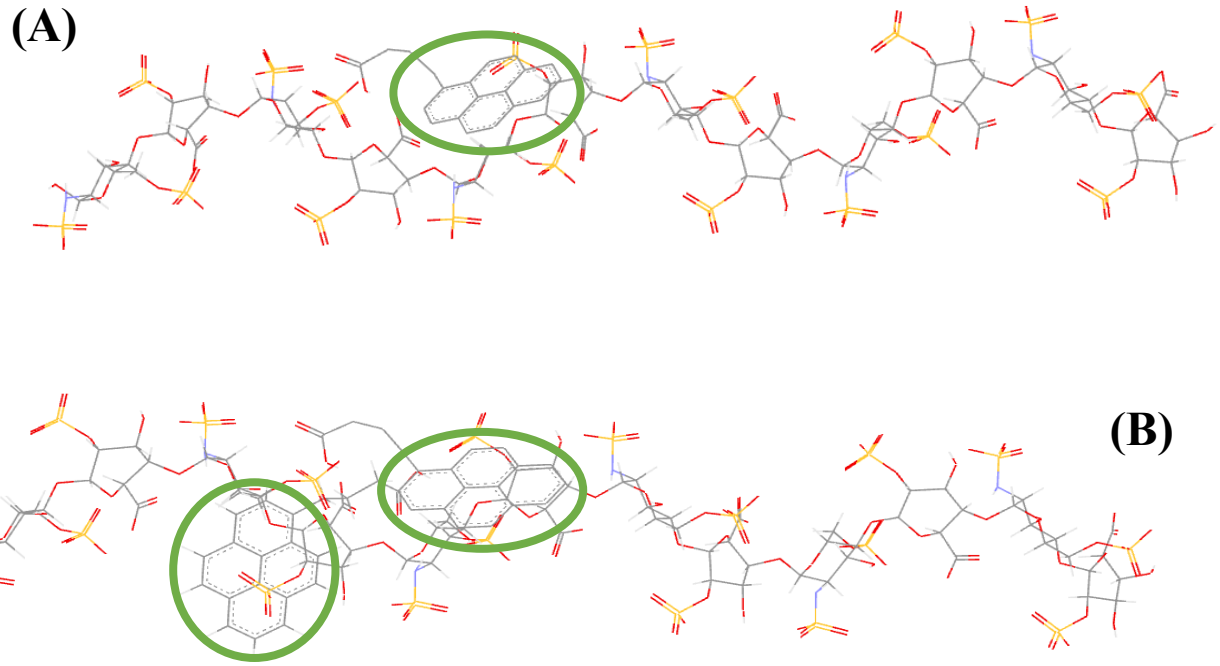

Figure. S34 Energy-optimized docking configuration of heparin and pyrene butyric acid, (A).1:1, (B).1:2, heparin/pyrene butyric acid

Results and discussion:

Detection Mechanism:

Steady-state emission and anisotropy of DPH:

We have analyzed steady-state emission and anisotropy measurements using DPH as a probe to understand the nature of the nanoGUMBOS microenvironments. The results show a significant increase in intensity and a spectral shift when DPH occupies the hydrophobic domains of the nanoGUMBOS. As illustrated in Fig. S35A, the emission intensity increases remarkably with a blue shift in the presence of nanoGUMBOS. With the addition of heparin, the emission intensity continues to grow with a blue shift; however, addition of protamine does not affect the fluorescence intensity. This phenomenon suggests that DPH is situated in a more hydrophobic medium.[42,43] The steady-state anisotropy of DPH in nanoGUMBOS increases with heparin, but the anisotropy slightly decreases with the addition of protamine (Fig. S36C).

Effect of SDBS and SDS on nanoGUMBOS:

To further understand the impact of SDBS on nanoGUMBOS, we investigated the steady-state emission and anisotropy of DCM and DPH in nanoGUMBOS in the presence of SDBS and CTAB. The fluorescence intensity of DCM in nanoGUMBOS is found to increase, but with SDBS addition, intensity decreases with a blue shift; with further addition of CTAB results in no significant change (Fig. S36B) in fluorescence. The anisotropy value of DCM in nanoGUMBOS gradually increases with the addition of SDBS and CTAB (Fig. S36C). The fluorescence intensity changes for DPH are challenging to interpret due to the same excitation wavelength. Still, the anisotropy study shows an increase with SDBS and a subsequent decrease with CTAB, which matches the anisotropy values observed in nanoGUMBOS (Fig. S36F). In DLS studies, the size of nanoGUMBOS decreases in the presence of SDBS and CTAB (Fig. S36I).

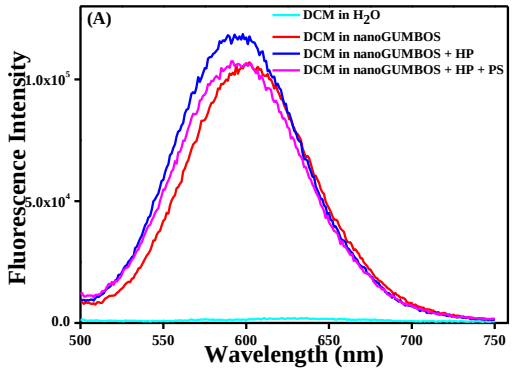

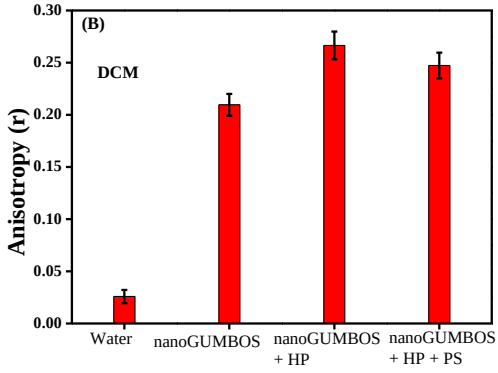

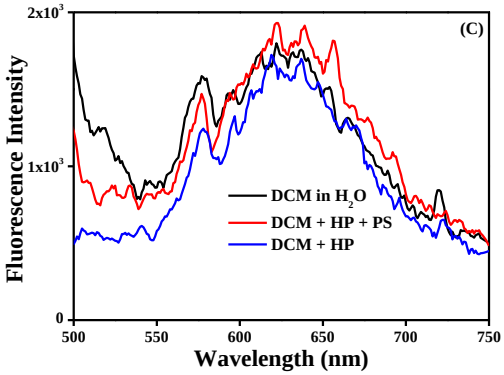

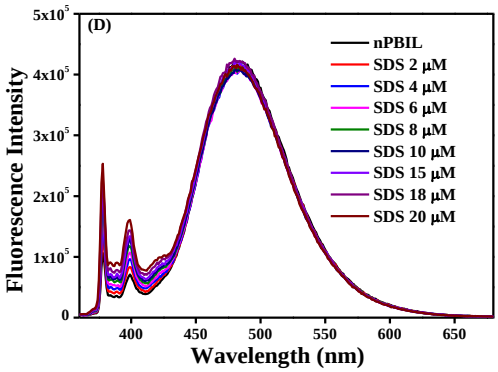

Fig. S35 (A). Fluorescence spectra of DCM (5µM) (λ_{ex}:480 nm) in presence of nanoGUMBOS, heparin, protamine; (B). Anisotropy of DCM in presence of nanoGUMBOS, heparin, protamine; (C). Fluorescence spectra of DCM in presence of heparin and protamine; (D). Fluorescence spectra of nanoGUMBOS in presence of SDS

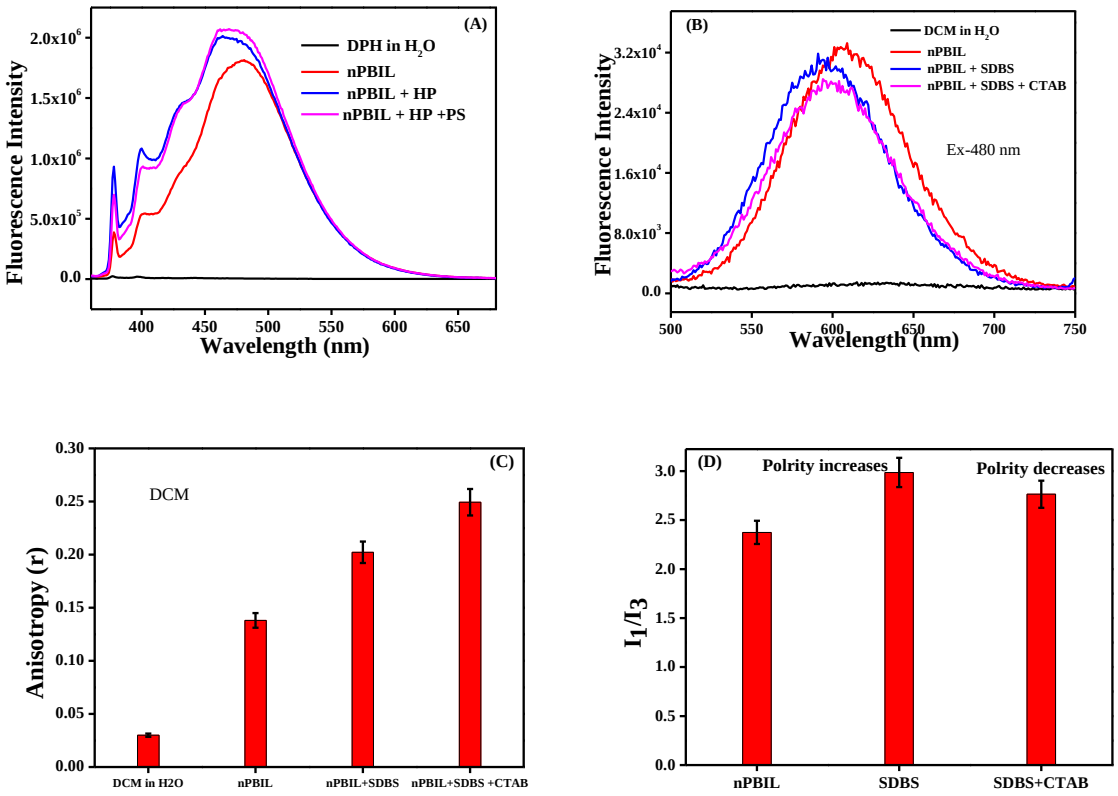

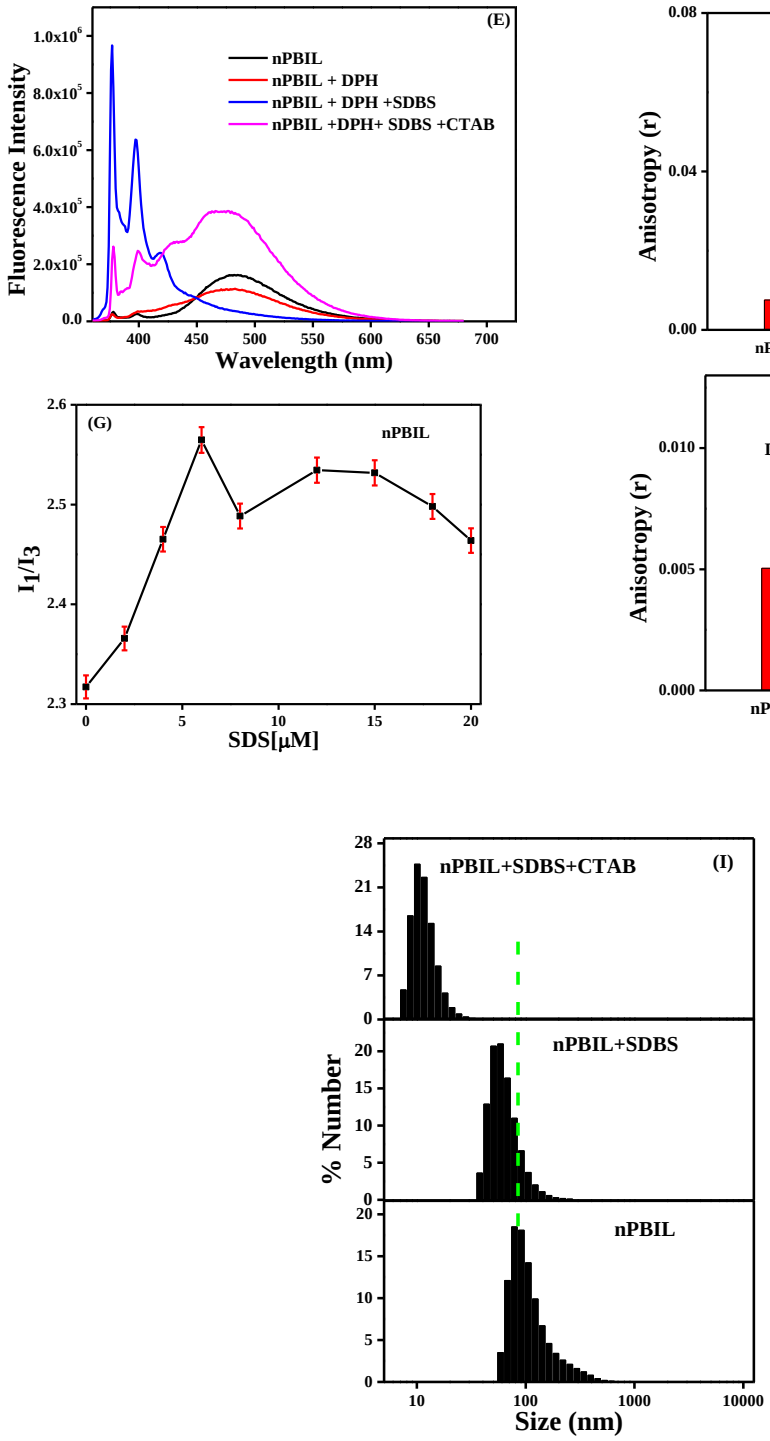

Figure. S36 (A). Fluorescence spectra of DPH in nPBIL in presence of heparin and protamine; (B). Fluorescence spectra of DCM in nPBIL in presence of SDBS and CTAB; (C). Anisotropy of DCM in nPBIL in presence of SDBS and CTAB; (D). I_1/I_3 ratio change of nPBIL in presence of SDBS and CTAB; (E). Fluorescence spectra of DPH in nPBIL in presence of SDBS and CTAB; (F). Anisotropy of DPH in nPBIL in presence of SDBS and CTAB; (G). I_1/I_3 ratio change of nanoGUMBOS with the addition of SDS; (H). Anisotropy of DPH in presence of

nanoGUMBOS, heparin, protamine; (I). DLS spectra of nanoGUMBOS in presence of SDBS and CTAB.

Table: S2 Fluorescence decay parameters of nPBIL (20 μg/mL) in presence heparin (λ_{ex}:295 nm, λ_{em}:377 nm)

Sample	α_1	α_2	α_3	τ_1	τ_2	τ_3	$\langle\tau\rangle$ **(ns)**[a]	χ^2
nPBIL	0.56	0.41	0.03	0.37	2.39	33.07	2.04	1.17
HP 2 μg/mL	0.52	0.31	0.17	0.47	3.24	36.93	7.56	1.14
HP 5 μg/mL	0.47	0.30	0.23	0.47	3.29	38.12	10.09	1.15
HP 10 μg/mL	0.43	0.27	0.30	0.29	2.96	39.03	12.63	1.15
HP 15 μg/mL	0.44	0.23	0.33	0.20	2.99	40.39	14.09	1.13
HP 20 μg/mL	0.44	0.21	0.35	0.19	2.99	40.37	15.04	1.14

Table: S3 Fluorescence decay parameters of nPBIL (20 μg/mL) in the presence of heparin (λ_{ex}:375 nm, λ_{em}:480 nm)

Sample	**α_1**	**α_2**	**α_3**	**τ_1**	**τ_2**	**τ_3**	**$<\tau>$(ns)[a]**	**χ^2**
nPBIL	-0.31	0.36	0.95	0.89	7.88	35.43	36.22	1.06
HP 1 μg/mL	0.22	0.12	0.65	1.89	9.04	39.03	27.03	1.10
HP 3 μg/mL	0.29	0.21	0.50	0.72	4.21	39.45	20.90	1.14
HP 5 μg/mL	0.28	0.32	0.40	0.31	2.62	39.77	16.54	1.14
HP 8 μg/mL	0.29	0.39	0.32	0.35	2.59	40.62	14.02	1.07
HP 10 μg/mL	031	0.41	0.28	0.35	2.54	41.31	12.79	1.05
HP 13 μg/mL	0.34	0.41	0.25	0.35	2.43	42.12	11.71	1.13
HP 16 μg/mL	0.35	0.42	0.23	0.34	2.47	42.91	10.96	1.12
HP 18 μg/mL	0.36	0.42	0.22	0.33	2.45	43.33	10.47	1.08
HP 20 μg/mL	0.42	0.40	0.18	0.22	2.38	43.34	9.17	1.11

a (% of error): ± 5%, χ^2 → Goodness of fitting

Table: S4 Lifetime value of nPBIL-heparin (HP) in the presence of different added concentration protamine sulfate (PS) (λ_{ex}:295 nm, λ_{em}:377 nm)

Sample	α_1	α_2	α_3	τ_1	τ_2	τ_3	$\langle\tau\rangle^a$	χ^2
nPBIL	0.56	0.41	0.03	0.37	2.39	33.06	2.04	1.11
HP 20 µg/mL	0.45	0.20	0.35	0.68	4.82	66.54	24.66	1.05
PS 1 µg/mL	0.42	0.21	0.37	0.80	5.89	70.11	27.63	1.07
PS 3 µg/mL	0.45	0.24	0.31	0.61	5.06	59.69	20.32	1.08
PS 5 µg/mL	0.44	0.26	0.30	0.68	5.41	60.81	19.77	1.06
PS 8 µg/mL	0.46	0.29	0.25	0.67	5.56	57.68	16.23	1.04
PS 12 µg/mL	0.49	0.32	0.19	0.56	5.21	47.48	10.58	1.10
PS 16 µg/mL	0.63	0.33	0.04	0.93	4.68	41.56	3.86	1.06
PS 20 µg/mL	0.68	0.29	0.03	1.28	4.92	36.62	3.46	1.07
PS 22 µg/mL	0.66	0.31	0.03	1.08	4.38	29.98	3.16	1.07
PS 25 µg/mL	0.73	0.24	0.03	1.05	4.05	37.17	2.82	1.09

Table: S5 Lifetime value of nPBIL-heparin system in the presence of different added concentration of protamine sulfate (PS) (λ_{ex} :375 nm, λ_{em} :480 nm)

Sample	α_1	α_2	α_3	τ_1	τ_2	τ_3	$<\tau>^a$	χ^2
nPBIL	-0.06	0.39	0.67	0.94	8.23	33.34	25.53	1.11
Hep 20 μg/mL	0.47	0.24	0.29	1.26	6.80	36.39	12.70	1.12
PS 1 μg/mL	0.47	0.22	0.31	1.61	6.02	33.31	12.53	1.05
PS 3 μg/mL	0.55	0.15	0.30	2.16	9.86	36.12	13.43	1.00
PS 5 μg/mL	0.34	0.31	0.35	1.79	8.30	32.15	14.32	1.08
PS 8 μg/mL	0.40	0.26	0.34	1.27	7.37	37.24	15.14	1.13
PS 12 μg/mL	0.38	0.24	0.38	1.33	7.28	37.03	16.28	1.10
PS 16 μg/mL	0.36	0.24	0.40	1.20	7.62	37.53	17.39	1.10
PS 20 μg/mL	0.22	0.24	0.54	1.31	9.94	35.59	21.75	1.09
PS 22 μg/mL	0.14	0.31	0.55	1.61	9.97	34.29	22.13	1.09
PS 25 μg/mL	0.14	0.29	0.57	3.32	10.5	36.84	24.54	1.12

a (% of error): ± 5%, χ^2 ⟶ Goodness of fitting

Table.S6 Detection of heparin in 20 μg/mL normal human serum albumin with nanoGUMBOS

[Recovery (%) = (added/found) × 100%]

Sl.No.	**Added (μg/mL)**	**Found (μg/mL)**	**Recovery (%)**
1	0.55	0.58	94.82
2	1.57	1.49	104.73
3	2.85	2.9	98.28
4	3.73	3.69	101.08

5	5.34	5.26	101.52
6	6.89	6.85	100.58
7	8.85	8.75	101.14
8	10.6	10.45	101.43
9	14.7	14.65	100.34
10	17.65	17.45	101.14
11	18.95	18.85	100.53

Table. S7 Summary of typical heparin sensors reported in literature

Mechanism	**Response range**	**LOD**	**Evaluation in human serum albumin matrix (%)**	**Ref.**
1.Ratiometric fluorescence	0.048−0.42 U/mL (0.4−3.5 μM)	6 mU/mL (50 nM)		1
2. Turn-off phosphorescence	0.05−1.4 U/mL	0.021 U/mL		2
3. Turn-on fluorescence	0.09−0.9 U/mL	0.00132 U/mL		3
4. Turn-on scattering, fluorescence and absorption	0.001−0.15 U/mL (8.3 × 10−3 −1.25 μM)	5.0 × 10−4 U/mL (4.2 × 10−3 μM)		4

5. Aggregation induced emission	0−28 000 nM	NA		5
6. Turn-off fluorescence	10−1000 nM	4 nM		6
7. Turn-off fluorescence	0.004−1.6 μg/mL (0.24−96.96 nM)	0.0013 μg/mL 0.08 nM		7
8. Aggregation induced emission	40−80 000 nM	40 nM		8
9. Aggregation induced emission	0−700 nM	30 nM		9
10. Turn-off gold nanorod	0.02−0.28 μg/mL (0.012−16.97 nM)	5 ng/mL (0.303 nM)		10
11. Turn-on Phosphorescence	1000−4000 nM	50 nM		11
12. Turn-on fluorescence	0−1.76 U/mL	0.046 U/mL		12

13. Aggregation induced emission	1000−10 000 nM	23 nM	Yes	13
14. AIEgen turn-off fluorescence	0.08–8 μg/mL	37 ng/mL	Yes (1%)	14
15.Turn-off fluorescence	0-49 ng/mL	2.4 ng/mL	Yes (1%)	15
16.Turn-off fluorescence	14.8 -148 nM	15 nM	Yes (1%)	16
17.Ratiometric fluorescence	10-100 nM	8.5 nM	Yes (10%)	17
18.Turn-on fluorescence	0-15 μg/mL	7.56 ng/mL	Yes (0.02)	18
19.Turn-on fluorescence	0-4.0 μM	4 nM	Yes (1%)	19
20.Turn-on fluorescence	0-10 μM	0.08 μM	Yes (1%)	20
21.Turn-on fluorescence	36-180 ng/mL	1.53 ng/mL	Yes (1%)	21
22.Turn on fluorescence	0-2 μg/mL	35.89 ng/mL	NO	22
23.Turn on fluorescence	0-1200 ng/mL	30 ng/mL	Yes (5%)	23
24.Turn on fluorescence	0-13 μM	34 nM	Yes (1%)	24

26.Turn on fluorescence	0-6 µg/mL	5.9 ng/mL	Yes (10%)	25
27.Ratiometric fluorescence (nanoGUMBOS)	0-20 µg/mL	2.01± 10% ng/mL	Yes (20%)	This work

Table. S8 Summary of Typical protamine sensors reported in literature

Mechanism	**Ratiometric**	**LOD**	**Evaluation in human serum matrix**	**Ref.**
1. HPLC	-	0.015 mg /mL	No	26
2.Electrochemistry	-	2.0 µg /mL	No	27
3. Fluorimetry	NO	2.2 ng /mL	No	28
4. Colorimetry and fluorimetry	NO	0.1 µg /mL	No	29
5. Fluorimetry	NO	1 ng/mL	Yes	30
6. Fluorimetry	NO	23.4 ng /mL	Yes	31
7.Fluorimetry	NO	0.4 mg/ mL	Yes	32
8. Fluorimetry	NO	0.13 µg /mL	Yes	33
9. Fluorimetry and colorimetry	Yes	31.5 ± 4.1 ng/ mL	Yes	34
10.Fluorimetry	NO	54.9 nM	Yes	35

11. Fluorimetry(nanoGUMBOS)	Yes	4.6 ± 10% ng/mL	Yes (20%)	This work

References

1.Yang, M. D.; Chen, J.; Zhou, H. P.; Li, W. Y.; Wang, Y.; Li, J. M.; Zhang, C. Y.; Zhou, C. B.; Yu, C. Polycation-induced benzoperylene probe excimer formation and the ratiometric detection of heparin and heparinase. Biosens. Bioelectron. 2016, 75, 404−410

2. Zhang, Z. F.; Miao, Y. M.; Zhang, Q. D.; Lian, L. W.; Yan, G. Q. Selective room temperature phosphorescence detection of heparin based on manganese-doped zinc sulfide quantum dots/Polybrene self-assembled nanosensor. Biosens. Bioelectron. 2015, 68, 556−562.

3. Liu, J. S.; Liu, G. N.; Liu, W. X.; Wang, Y. R. Turn-on fluorescence sensor for the detection of heparin based on rhodamine B-modified polyethyleneimine-graphene oxide complex. Biosens. Bioelectron. 2015, 64, 300−305

4. Ling, Y.; Gao, Z. F.; Zhou, Q.; Li, N. B.; Luo, H. Q. Multidimensional optical sensing platform for detection of heparin and reversible molecular logic gate operation based on the phloxine B/ polyethyleneimine system. Anal. Chem. 2015, 87, 1575−1581

5. Chen, L. J.; Ren, Y. Y.; Wu, N. W.; Sun, B.; Ma, J. Q.; Zhang, L.; Tan, H. W.; Liu, M. H.; Li, X. P.; Yang, H. B. Hierarchical self-assembly of discrete organoplatinum (II) metallacycles with poly-saccharide via electrostatic interactions and their application for heparin detection. J. Am. Chem. Soc. 2015, 137, 11725−11735

6. Hung, S. Y.; Tseng, W. L. A polyadenosine-coralyne complex as a novel fluorescent probe for the sensitive and selective detection of heparin in plasma. Biosens. Bioelectron. 2014, 57, 186−191

7. Zhao, J. N.; Yi, Y. H.; Mi, N. X.; Yin, B. D.; Wei, M. J.; Chen, Q.; Li, H. T.; Zhang, Y. Y.; Yao, S. Z. Gold nanoparticle coupled with fluorophore for ultrasensitive detection of protamine and heparin. Talanta 2013, 116, 951−957

8. Chen, D. Y.; Shi, J. B.; Wu, Y. M.; Tong, B.; Zhi, J. G.; Dong, Y. P. An AIEE polyelectrolyte as a light-up fluorescent probe for heparin sensing in full detection range. Sci. China: Chem. 2013, 56, 1239− 1246

9. Xu, B. W.; Wu, X. F.; Li, H. B.; Tong, H.; Wang, L. X. Fluorescent detection of heparin by a cationic conjugated polyfluorene probe containing aggregation-induced emission units. Polymer 2012, 53, 490−494

10. Fu, X. L.; Chen, L. X.; Li, J. H.; Lin, M.; You, H. Y.; Wang, W. H. Label-free colorimetric sensor for ultrasensitive detection of heparin based on color quenching of gold nanorods by graphene oxide. Biosens. Bioelectron. 2012, 34, 227−231

11. Yan, H.; Wang, H. F. Turn-on room temperature phosphorescence assay of heparin with tunable sensitivity and detection window based on target-induced self-assembly of polyethyleneimine capped Mn-doped ZnS quantum dots. Anal. Chem. 2011, 83, 8589−8595

12. Cai, L. P.; Zhan, R. Y.; Pu, K. Y.; Qi, X. Y.; Zhang, H.; Huang, W.; Liu, B. Butterfly-shaped conjugated oligoelectrolyte/graphene oxide integrated assay for light-up visual detection of heparin. Anal. Chem. 2011, 83, 7849−7855

13. Wang, M.; Zhang, D. Q.; Zhang, G. X.; Zhu, D. B. The convenient fluorescence turn-on detection of heparin with a silole derivative featuring an ammonium group. Chem. Commun. 2008, 37, 4469−4471

14. R. Jiang, S. Zhao, L. Chen, M. Zhao, W. Qi, W. Fu, L. Hu, Y. Zhang, Fluorescence detection of protamine, heparin and heparinase II based on a novel AIE molecule with four carboxyl, Int. J. Biol. Macromol. 156 (2020) 1153–1159.

15.G.H. Aryal, G.R. Rana, F. Guo, K.W. Hunter, L. Huang, Heparin sensing based on multisite-binding induced highly ordered perylene nanoaggregates, Chem. Commun. 56 (87) (2020) 13437–13440.

16. P. Jana, M. Radhakrishna, S. Khatua, S. Kanvah, A ‘‘turn-off’’ red-emitting fluorophore for nanomolar detection of heparin, Phys. Chem. Chem. Phys. 20 (19) (2018) 13263–13270.

17. W. Gong, S. Wang, Y. Wei, L. Ding, Y.u. Fang, A pyrene-based fluorescent sensor for ratiometric detection of heparin and its complex with heparin for reversed ratiometric detection of protamine in aqueous solution, Spectrochim. Acta, Part A 170 (2017) 198–205.

18.J. Zheng, J. Cao, Y. Tu, S. Wang, Detection of heparin by fluorescent sensor based on naphthalimide derivatives in human serum, Dyes Pigm. 181 (2020)

19. J. Cui, S. Zang, W. Shu, H. Nie, J. Jing, X. Zhang, highly sensitive and selective detection of heparin in serum based on a long-wavelength tetraphenylethylene-cyanopyridine aggregation-induced emission luminogen, Anal. Chem. 92 (10) (2020) 7106–7113.

20.S. Yang, T. Gao, J. Dong, H. Xu, F. Gao, Q. Chen, Y. Gu, W. Zeng, A novel watersoluble AIE-based fluorescence probe with red emission for the sensitive detection of heparin in aqueous solution and human serum samples, Tetrahedron Lett. 58 (37) (2017) 3681–3686.

21.J. Zheng, T. Ye, J. Chen, L.i. Xu, X. Ji, C. Yang, Z. He, Highly sensitive fluorescence detection of heparin based on aggregation-induced emission of a tetraphenylethene derivative, Biosens. Bioelectron. 90 (2017) 245–250.

22.Y. Gao, K. Wei, J. Li, Y. Li, J. Hu, A facile four-armed AIE fluorescent sensor for heparin and protamine, Sens. Actuators, B (2018) 408–414.

23.Q. Kang, Y. Xiao, W. Hu, Y. Wang, Smartly designed AIE triazoliums as unique targeting fluorescence tags for sulfonic biomacromolecule recognition via 'electrostatic locking', J. Mater. Chem. C 6 (46) (2018) 12529–12536

24.N.H. Mudliar, P.K. Singh, Emissive H-aggregates of an ultrafast molecular rotor: a promising platform for sensing heparin, ACS Appl. Mater. Interfaces 8 (46) (2016) 31505–31509.

25. Xiaomeng Liang, Hailiang Nie, Chunliu Yang, Zhenguang Wang, Jie Bai, Hongyuan Yan. A cationic aggregation-induced emission luminogen for colorimetric and fluorimetric detection of heparin with a dual-read approach, stability and applicability in a 10% serum matrix. Journal of Molecular Liquids 343 (2021) 117585

26. D. Awotwe-Otoo, C. Agarabi, P.J. Faustino, M.J. Habib, S. Lee, M.A. Khan, et al., Application of quality by design elements for the development and optimization of an analytical method for protamine sulfate, J. Pharm. Biomed. Anal. 62 (2012) 61–67

27. S. Pang, S. Liu, X. Su, A fluorescence assay for the trace detection of protamine and heparin, RSC Adv. 4 (2014) 25857–25862

28. Z. Yao, W. Ma, Y. Yang, X. Chen, L. Zhang, C. Linc, et al., Colorimetric and fluorescent detection of protamines with an anionic polythiophene derivative, Org. Biomol. Chem. 11 (2013) 6466–6469.

29. A.A. Ensafi, N. Kazemifard, B. Rezaei, A simple and rapid label-free fluorimetric biosensor for protamine detection based on glutathione-capped CdTe quantum dots aggregation, Biosens. Bioelectron. 71 (2015) 243–248

30. Y. Gao, K. Wei, J. Li, Y. Li, J. Hu, A facile four-armed AIE fluorescent sensor for heparin and protamine, Sensors Actuators B Chem. 277 (2018) 408–414.

31.G. Guan, J. Sha, D. Zhu, Heparin-MPA dual modified CdS quantum dots used as a simple and rapid label-free fluorescent sensor for protamine and hemin detection, Microchem. J. 133 (2017) 391–397.

32.H. Li, X. Yang, Bovine serum albumin-capped CdS quantum dots as inner-filter effect sensor for rapid detection and quantification of protamine and heparin, Anal. Methods 7 (2015) 8445–8452.

33.J. Liu, M. Xu, B. Wang, Z. Zhou, L. Wang, Fluorescence sensor for detecting protamines based on competitive interactions of polyacrylic acid modified with sodium 4-amino-1-naphthalenesulfonate with protamines and aminated graphene oxide, RSC Adv. 7 (2017) 1432–1438.

34.Y. Liu, F. Zhang, X. He, P. Ma, Y. Huang, S. Tao, et al., A novel and simple fluorescent sensor based on AgInZnS QDs for the detection of protamine and trypsin and imaging of cells, Sensors Actuators B Chem. 294 (2019) 263–269

35. Rakesh Biswas and Supratim Banerjee., Luminescence Sensing of Biomacromolecules Heparin andProtamine in 100% Human Serum and Plasma by Supramolecular Polymeric Assemblies. *Biomacromolecules* 2023, 24, 766−774